Geotechnical Journal

Sri Lankan Geotechnical Society
C/o National Building Research Organisation
99/1, Jawatta Road, Colombo 5
Sri Lanka

ISSN-1391-6149

GEOTECHNICAL JOURNAL

CONTENT

Back analysis of slope failure at Welipanna, Southern Express Way **1-10**
I.A.N.D Idirimanna and S.A.S. Kulathilaka

A laboratory-scale numerical study of CO_2 flow through coal under down-hole stress conditions: Application to CO_2 storage **11-21**
A.S. Ranathunga, M.S.A. Perera and P.G. Ranjith

Effect of salinity on the rate of consolidation of Sri Lankan soft peat **22-29**
T. Jayasinghe, U.P. Nawagamuwa and K.H.S.S. De Silva

Study of pullout resistance of soil nails in tropical residual soils **30-40**
W.E.P. Ranjan Kumara and S.A.S. Kulathilaka

Back analysis of slope failure at Welipanna, Southern Express Way

I.A.N.D Idirimanna[1] and S.A.S. Kulathilaka[2]

1 *Landslide Research and Risk Management Division, NBRO*
2 *Department of Civil Engineering, University of Moratuwa, Sri Lanka*

ABSTRACT: Slope failures due to excessive rainfall are a common geotechnical hazard in tropical countries where residual soils are abundant. Heavy infiltration of rainwater causes destruction of matric suctions, development of perched water table and rise of ground water table eventually leading to failure. Sri Lankan residual soils formed by weathering of metamorphic rocks have significant abrupt variations in engineering characteristics due to variations in mineralogical composition of the parent rock and weathering under humid heavy rainfall conditions at high temperatures. Joints in the parent rock are present as relict joints in the parent rock adding further complications. This paper presents the back analysis of a failure occurred in a cut slope at Welipanna in Southern expressway. Infiltration was modelled with GEOSLOPE SLOPE/W software using the SWCC and permeability function derived for the soil obtained from the site. In view of the many uncertainties present, the back analysis was done in the form a parametric study considering the possible presence of systems of relict joints and possible defects in the surface drainage system. The results also revealed that if the drainage system was in perfect working order this failure would not have occurred. The study revealed that the rise of ground water table is quite significant at toe of the slope. Hence it is recommended to have sub horizontal drains at the toe level even if the ground water table is found to be lower than the toe level in general.

Keywords: *Infiltration, Matric Suction, Relict Joints, Slope Stability*

1. INTRODUCTION

Rainfall-induced slope failure creates one of the most common geotechnical hazards in tropical regions such as Sri Lanka. The intense rainfall is the major triggering factor under these conditions. Safety margins of these slopes are high during the periods of dry weather due to the prevailing matric suctions. As a result of heavy rainfall, significant infiltration takes place and soil at the surface is getting nearly saturated. With rainfall of greater intensity perched water table conditions can also develop. The wetting front that progresses downwards with the prolonged rainfall will cause a rise of the ground water table. Towards the toe of the slope the infiltration would cause much greater destruction of the matric suction profile and greater rise of ground water table. These events would lead to a significant reductions in the safety margins of the slope and could trigger a failure (Sujeevan and Kulathilaka 2011).

A failure occurred in a cut slope at 42+340 to 42+400 in Welipanna in the southern expressway on 2nd November 2012, after a rainfall that continued for several days. The site is located in between Dodangoda and Walipanna interchanges in the Kaluthara district. The slope is a terraced slope with an average inclination of 40^0. Subsequently, the slope was rectified by combined measures of; surface and sub surface drainage, slope reinforcement and toe retaining structures.

The objective of this study is to back analyses the failure and identify the reasons. Many findings of the rectification process were used in the study. In view of many uncertainties, prevailing the back analysis was done in the form of a parametric study.

2. GEOLOGY AND SUBSOIL PROFILE

The slope is formed of residual soils where the parent rock is metamorphic. Type of the bedrock is garnet biotite gneissic. Outcrops of the bedrock can be seen at the top of the slope at 42+350 to 42+400. The bedrock is dipping into the slope at a very steep (80^o) angle. The ground water table was above the road level according to the continuous water level measurements.

Due to weathering under high ambient temperature and high rainfall conditions and the differences in the mineralogical structure in the parent rock the weathered product is highly variable. As a result, boudinage structures - rocks with no or very slight weathering can be seen embedded in a matrix of soil. These boudinage structures were identified during the drilling for soil nailing in the rectification process. A typical condition encountered during drilling is presented in Figure 1.

Five different joint systems were identified in the rocks in the area. As such, relict joints can be expected in the residual soil. During the drilling for soil nailing for rectification, the water trapped in the relict joints released under very high pressure covering the workers in mud (Figure 2). This confirms that there is water under high pressure in the relict joints. This water will disperse into the soil around making it saturate. The presence of pore water under higher pressure itself will have adverse effects on stability.

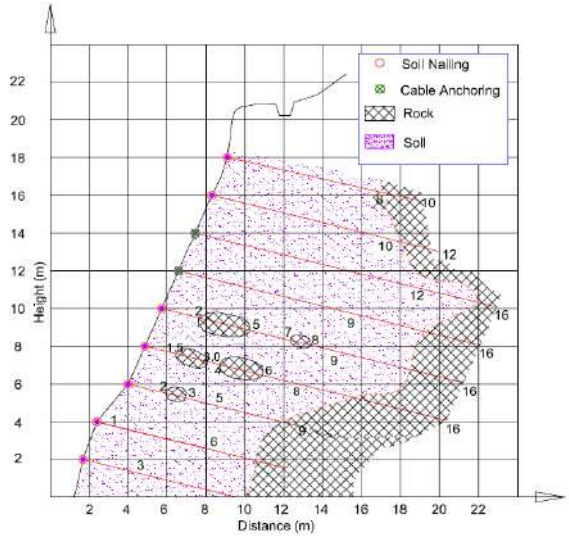

Figure 1: Typical condition with boudinage structures encountered during drilling

Figure 2: Water oozing out of relict joints during drilling and covering the workmen in mud

3. THE INITIAL DESIGN OF THE CUT SLOPE

During the constructions of STDP the hilly area in between the chain edges of 42+380 to 42+440 was subjected to deep cuts. Five boreholes were advanced and consolidated drained tri axial tests were performed on undisturbed samples obtained after saturation. The design shear strength parameters were assigned after

considering the; SPT N values, laboratory test results and the experience on similar type of soils. The main soil type is a Sandy Silt with Specific Gravity of 2.66 and dry density is 1210kg/m^3. Particle size distribution is presented in Figure 3. Index properties of the soil are summarized in Table 1. Shear strength parameters assigned are; c'=10 kN/m^2 and ϕ '=32^o. Slope was designed to cut the slope at the gradient of 1:1.2 keeping berms at every 7.5m height difference. This yielded a Factor of Safety of 1.2. There were five berms in the slope.

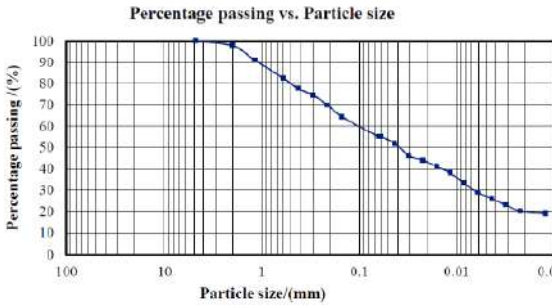

Figure 3: Particle size distribution for Sandy Sil , Vasanthan (2016)

Table 1: Summary of index property test for Sandy Silt

Sample No.	Classification		Liquid limit	Plastic limit	Plasticity index	Gravel (%)	Sand (%)	Silt (%)	Clay (%)
	BSCS	USCS							
Sample 2	MS	MH	54	43	11	2	43	35	20

In order to minimize the infiltration and the loss of matric suction or development of perched water table, surface drainage of the area had been well developed with concrete paved berm drains on each berm and cascade drains to collect water from berm drains and facilitate free flowing of rainfall runoff down the slope. Further, the slope is covered with grass to control the erosion (Figure 4). The grass cover also deflects the falling rain drops as runoff while minimizing infiltration.

Figure 4: Berm drains and cascade drains

4. NATURE OF FAILURE

After several days of rainfall a failure occurred in the slope up to the height of 3rd berm level. Landslide occurred over a length about 50m along the road and extends over a height of about 20 m. The slip surface is quite shallow.

On the day of failure, cracks appeared on the crown of the terraced slope around 9.30 am (Figure 5). The cracking of the cascade drain(undetected) just above this level and possible leakage of water to the slope for quite some time could also be seen. Below the level of the crack in the slope, the berm drains have also cracked. Cracks widened within the day and eventually failure occurred by 3 pm. The soil mass has been moved toward the carriageway and debris with an approximate flow length of 30 m from toe are accumulated on the 10m wide road reservation and whole road section towards the Galle (Figure 6). The road itself was not damaged, but rather had been covered by the debris of the slide. The affected segment of the road was about 70m long.

Figure 5: Initial Crack & downward movement of soil

5. POSSIBLE REASONS OF FAILURE

The failure that occurred in this slope was triggered by the excessive rainfall that prevailed in the area over the days preceding the failure. Some cracks that existed in the drainage system (cascade drains) could be detected only after the catastrophic failure. It was evident that significant infiltration has taken place due to the heavy rainfall. Water could have seeped into the soil through the cracks.

Zones of whitish feldspar rich clays could be identified at limited locations around the mid level of the left escarpment of the landslide scar. This weak material may also have contributed significantly to the failure. The shear strength of this material under saturated condition would be much lower than the saturated shear strength determined at the design stage.

The failure also has been facilitated further by excessive infiltration of rainwater into a system of adversely oriented relict joints. Relict joints would be filled with loose material /weak material. Water infiltrated into relict joints could facilitate saturation of the slope material. Further, there could have been pore pressure built up in relict joints as demonstrated by water oozing out at high pressure.

In such situations the sliding could take place at a shallow depth without the need of the ground water table rising to a higher level. The observation after the failure was similar. The debris were not having lot of moisture. However, just prior to the failure water getting released under high pressure or oozing out of water near the toe has been observed. This could be attributed to the perched water table condition developed closer to the toe of the slope which was confirmed during the back analysis.

6. RECTFICATION DESIGN

The drilled and grouted soil nails were constructed as the main stabilizing measure. The diameter of the drill holes were 125 mm. The reinforcement inserted were 25 mm and 32mm diameter tor steel bars. Soil nailing design involved nails of 16m length at the highest location. Later it was decided to use cable anchors in place of 16m long nails. The other nails were of length of 12m. Cable anchors were pre-tensioned to 180 kN. Thereafter all the nail heads and cable anchoring heads were connected by a system of beams and the complete surface was covered with sprayed concrete.

Surface drainage improvement was done by repairing all failed berm drains and cascade drains. To prevent the buildup of positive pore water pressures behind the concrete surface, short drains of length around 2.0m were provided in a grid of 1.5 X 1.5m. To minimize the rising of ground water table during heavy prolong rainfall and minimize the activation of deep seated slip surfaces, long drains of length around 12m were provided at 5m horizontal spacing. The location of soil nails, cable anchors and long horizontal drains are presented in the elevation diagram in Figure 6.

A gabion wall of height 4.5 was also needed at the toe to ensure stability. The improvement of the safety margin to a Factor of Safety of 1.390 with the proposed stabilizing measures is illustrated in Figure 7.

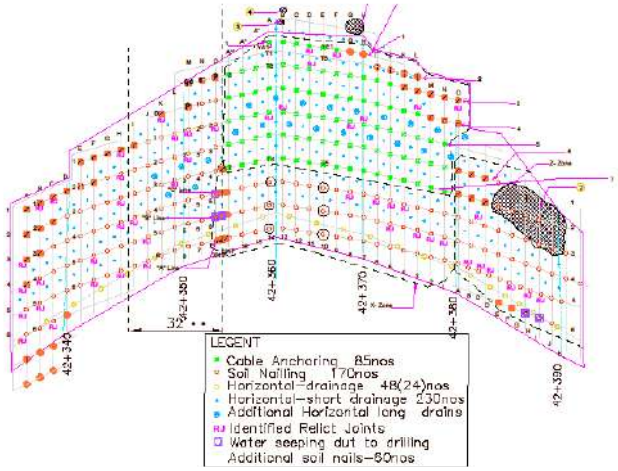

Figure 6: The location of soil nails, cable anchors and long horizontal drains

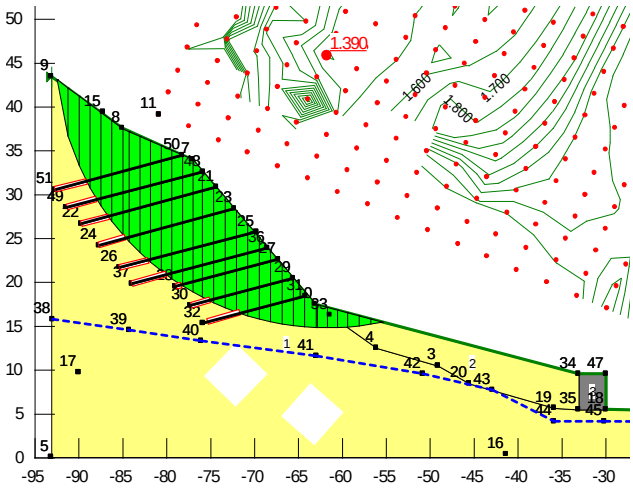

Figure.7: Proposed stabilization with soil nailing subsurface drainage and toe wall

7. BACK ANALYSIS OF SLOPE FAILURE

7.1 Preparation of Infiltration model

The rainfall data over a week preceding the failure were gathered from rain gauge stations closest to the location at Bombuwala and Baddegama. For the analysis, actual peak rainfall measured on 5 days preceding the failure was idealized and applied under appropriate slope boundary conditions. As Figure 8, rainfall was not extreme during the failure, but prolonged with low intensity, where maximum recorded rainfall was 7mm/hr.

Although there were boudinage structures identified during the rectification process, the slope was modeled to be made of a uniform residual soil (Sandy Silt) in this study.

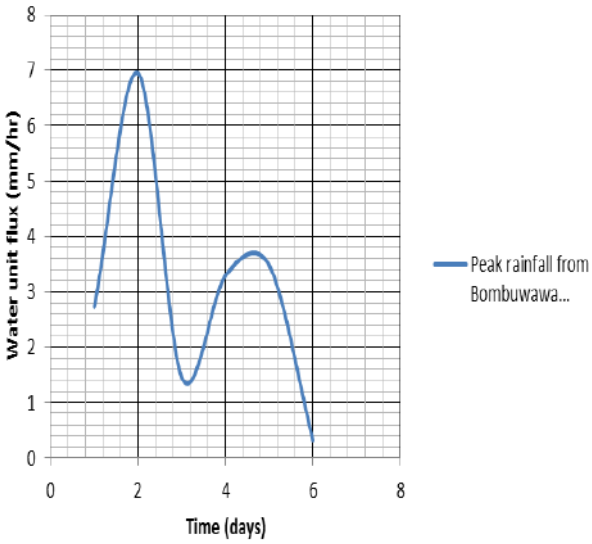

Figure 8: Peak rainfall from Bombuwawa and Beddegama Rain Gauges

Similar to the flow through a saturated soil, water flow through an unsaturated soil is generally governed by Darcy's law (Fredlund and Rahardjo - 1993). However, two major differences stand out:

(1) There exists a storage term which represents the variation of water content with matric suction; and
(2) The water coefficient of permeability depends strongly on matric suction.

It should be noted that no volume change in soil is considered during the infiltration process. The storage term in unsaturated flow is not a constant but dependent on the suction (or water content) and can be characterized by the Soil Water Characteristic curves (SWCC). Therefore, SWCC and water coefficient of permeability are the most important hydraulic properties for unsaturated soils.

Permeability function and soil water characteristic curve (SWCC) for the soil forming the slope were obtained through laboratory tests done by Vasanthan (2016). These information were not available at the time of the rectification design and a detailed infiltration study was not done there. The SWCC curve and the Permeability Function were determined by the method of continuous measurements with KU tensiometers (Vasanthan 2016). The curves are shown in Figure 9 and Figure 10 respectively. The matric suction profile that prevailed prior to the rainfall could not be obtained. As such, the negative pore water pressures were given a cutoff value of 100 kN/m^2 (as presented in the pore water pressure profiles in Figure 12 onward)

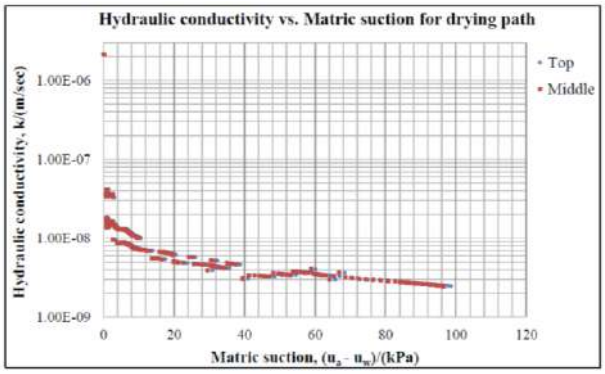

Figure 9.: K function used for the analysis, - Sandy Silt– drying path, Vasanthan (2016)

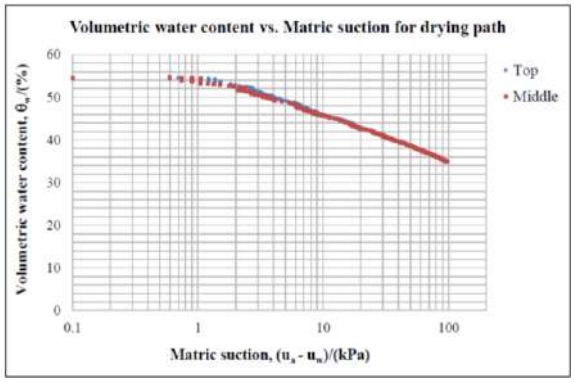

Figure 10: SWCC used for analysis - Sandy Silt drying path, Vasanthan(2016)

According to the Darcy-Buckingham equation, horizontal and vertical water flux (q_x and q_z) in unsaturated soil are expressed as follows:

$$q_x = -k(\psi)\left(\frac{\partial \psi}{\partial x}\right) \quad \text{Eq [1]}$$

$$q_z = -k(\psi)\left(\frac{\partial \psi}{\partial z} + 1\right) \quad \text{Eq [2]}$$

Where k(ψ) - hydraulic conductivity as a function of negative pore water pressure ψ.

The equation for continuity of water is expressed as

$$\frac{\partial \theta}{\partial t} = -\left(\frac{\partial q_x}{\partial x} + \frac{\partial q_z}{\partial z}\right) \quad \text{Eq [3]}$$

Where, t is time, Substituting Equation -1 and Equation -2 into Equation -3 yields the two-dimensional, vertical and horizontal flow equation for soil water (Richard's Equation):

$$\frac{\partial}{\partial z}\left(K(\psi)\frac{\partial \psi}{\partial z}\right) + \frac{\partial}{\partial x}\left(K(\psi)\frac{\partial \psi}{\partial x}\right) + \frac{\partial}{\partial z}\left(K(\psi)\right) = c(\psi)\frac{\partial \psi}{\partial t} \quad \text{Eq [4]}$$

Where $c(\psi) = \partial\theta / \partial\psi$ is the water capacity function defined as the slope of the SWCC.

These equations were solved using GEOSLOPE SEEP/W software solved with a finite element formulation adopting the SWCC and hydraulic conductivity functions presented here.

In view of the incompleteness of data such as details of systems of relict joints and antecedent matric suction, the back analysis was done in the form of a parametric study. Infiltration behavior of the slope was studied both with and without the presence of relict joints. These joints were assumed to be of width 100mm and filled with loose material. As there was evidence that surface drainage measures implemented were disturbed to some extent analysis were done both with and without the drainage measures. The parametric studies done could be summarized as;

(a) Infiltration analysis without surface drainage measures - Without relict joints and with relict joints
(b) Infiltration analysis with surface drainage measures - Without relict joints and with relict joints

7.2 Boundary conditions

Input parameters and boundary conditions were incorporated to the SEEP/W software to represent the actual seepage conditions of the slope and generate the rainwater infiltration model of slope as presented in Figure 11. Variation of rainfall intensity with time was applied to the soil surface of A-B, B-C and C-D. Zero total flux was applied to the side of the slope above the water table at A-G and D-E to simulate the non-lateral flowing of infiltrated water. Zero total flux was also applied to the bottom of the profile at F-H to simulate no flow of ground water to further down. Initial total heads, h_t, were applied at the sides of the slope below the water table at E-F and G-H, to maintain the minimum depth to ground water table.

7.3 Results of the Infiltration Analysis

The results of the infiltration analysis done for variable conditions mentioned above is presented for the idealized rainfall in the form of variation of pore water pressure distribution Vs depth for sections 1 and 2 of the slope idealized with the FE mesh in Figure 11. The assumed set of relict joints (when they are in use) and mesh is presented in Figure 12. Size of the element within the thin relict joints was made smaller to suit its width. As such, the size of the elements in the vicinity of the relict joint also had to be made to a smaller size to be compatible. Thus the number of elements in the finite element mesh corresponding to the case with relict joints is much larger.

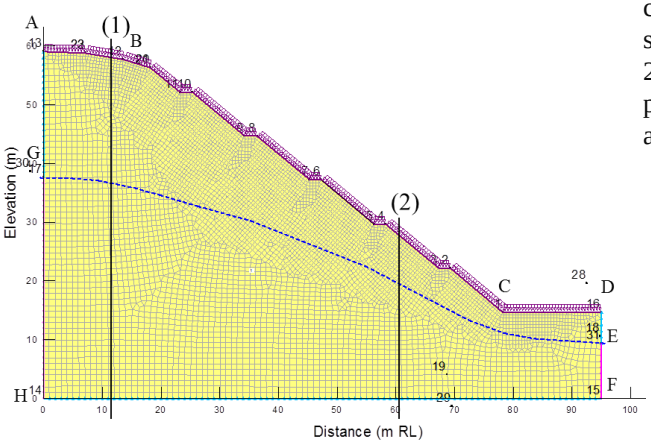

Figure. 11: Idealization of the Analyzed slope

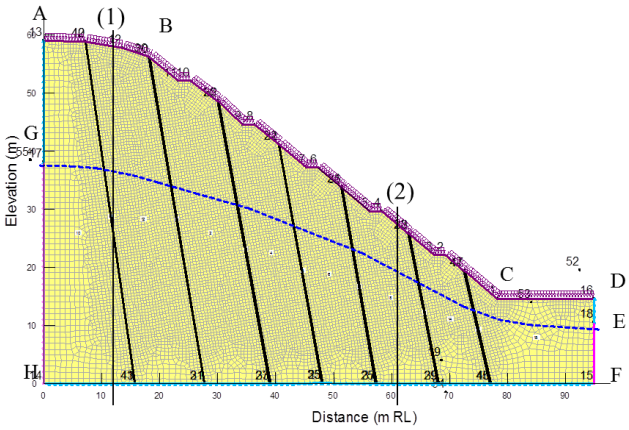

Figure 12: Slope with relict joints

7.3.1 Infiltration analysis without surface drainage measures

Analyses were done for the two conditions; with and without relict joints. The response of the slope when relict joints are not present is illustrated in Figure 13 and Figure 14. The result of the analysis shows that as rainfall continues the matric suction values are gradually diminished approaching zero and the process extends to greater depths with time(Figure 13). Water reaching deeper levels cause a rise of ground water table and this effect is more prominent towards bottom levels of the slope (Figure 14).

The response when relict joints are there is presented in Figure 15 and Figure 16. It is evident that the loss of matric suction and rise of ground water table is more significant when the relict joins are present. This is due to the highly permeable loose filling material in the relict joints which facilitates the penetration of water into the deeper levels of the slope without getting stagnant at the surface. Figure 17 illustrates that the infiltration through relict joints is much greater than the infiltration through soil slope. The arrow represents the intensity of the infiltration. When relict joins are not present, the excess rainfall that could not infiltrate further would contribute to runoff. The presence of water trapped under high pressure in relict joints was confirmed when water oozed out during the drilling for soil nailing in the rectification (Dhramasena et al 2015).This emphasizes that, the modeling of the presence of relict joints is a significant feature in the analysis.

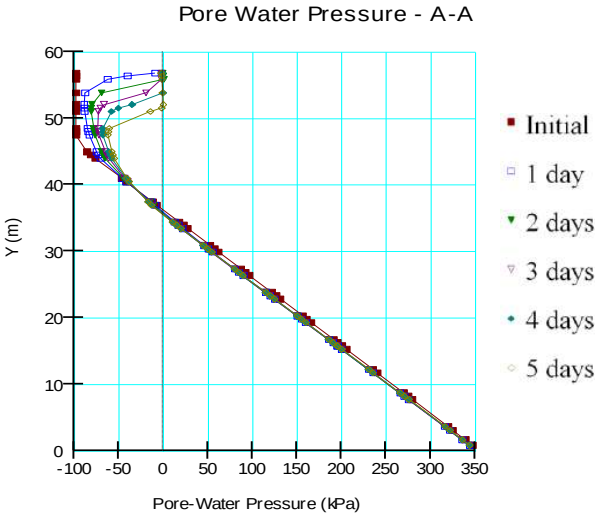

Figure 13: Pore water distribution vs depth in sections 1 for the slope without surface drainage measures, Without Relict joints

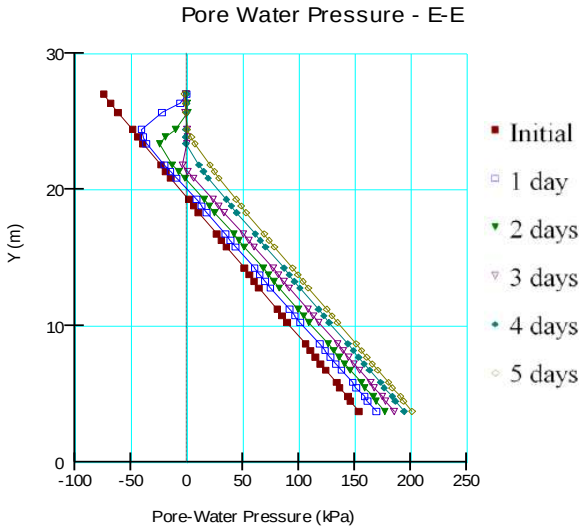

Figure 14: Pore water distribution vs depth in sections 2 for without surface drainage measures, Without Relict joints

The result of the analysis shows that as rainfall continues the matric suction values are gradually eliminated and pore water pressure become zero or just positive (negative pore water pressure). It reveals the development of thin perched water table at the surface. Infiltration into the relict joints is graphically illustrated in Figure 17.

As rainfall continues the loss of matric suction advances to greater depths. (The wetting front progresses downward). In the meantime the water table also moves upwards. Effect of progression of wetting front and the rise of ground water table is more

prominent towards bottom levels of the slope, in section 2.

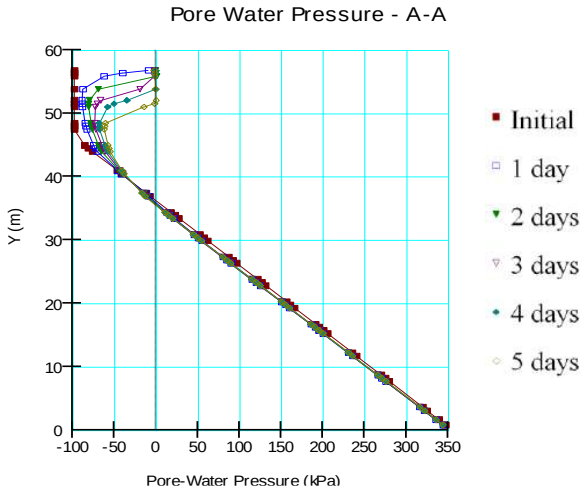

Figure 15: Pore water distribution vs depth in sections 1 for the slope without surface drainage measures – With Relict joints

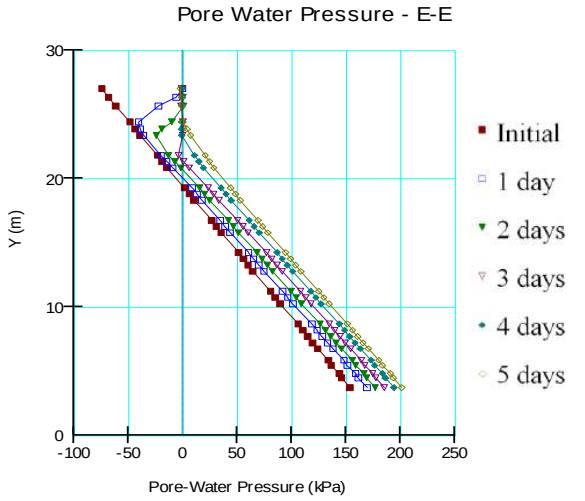

Figure 16: Pore water distribution vs depth in sections 2 for the slope without surface drainage measures – With Relict joints

7.3.2 Infiltration Analysis When Surface Drainage Measures are Present

The surface drainage of the cut slope had been enhanced by providing concrete paved berm drains and cascades for free flowing of water runoff from upper slope. Further, the slope is covered with grass to control erosion and minimize infiltration.

The influence of said drainage measures were modeled with the software SEEP/W by incorporating a 100mm thick layer of very low permeability 10^{-20} m/s over the berms simulating the concrete cover and a 100mm thick layer of low permeability 10^{-7}m/s over the slope surface

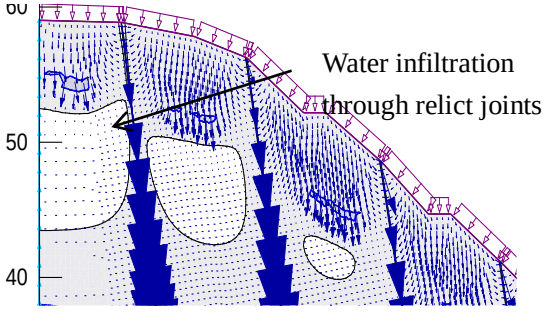

Figure 17: Rain infiltration through slope profile an relict joints

simulating the vegetation cover. The changes in the pore pressure regime for the Section 1and Section 2 for the case without relict joints is presented in Figure 18 and Figure 19 and for the case with relict joints is presented in Figure 20 and Figure 21 respectively.

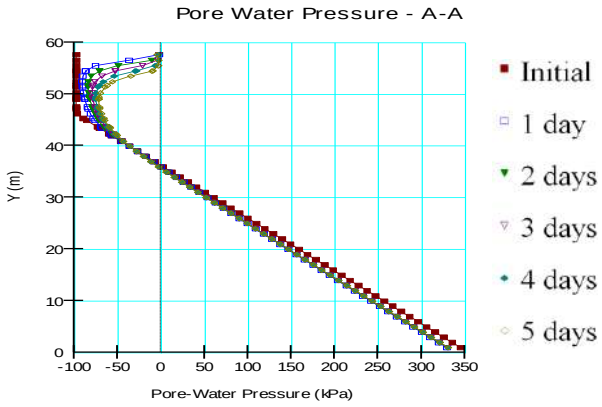

Figure 18: Pore water distribution vs depth in sections 1 for slope without relict joints and with surface drainage improvement (Permeability of vegetation layer = 10^{-7} m/s)

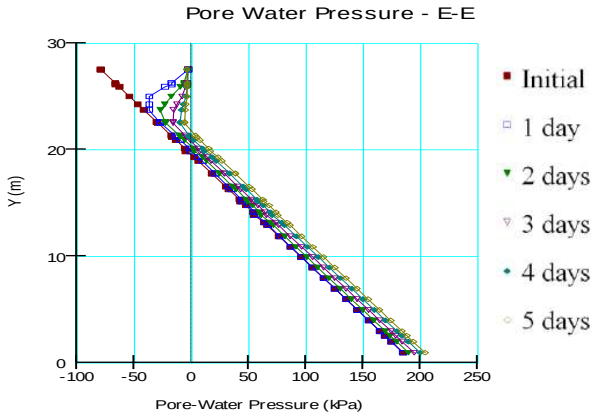

Figure 19: Pore water distribution vs depth in sections 2 for slope without relict joints and with surface drainage improvement (Permeability of vegetation layer= 10^{-7} m/s)

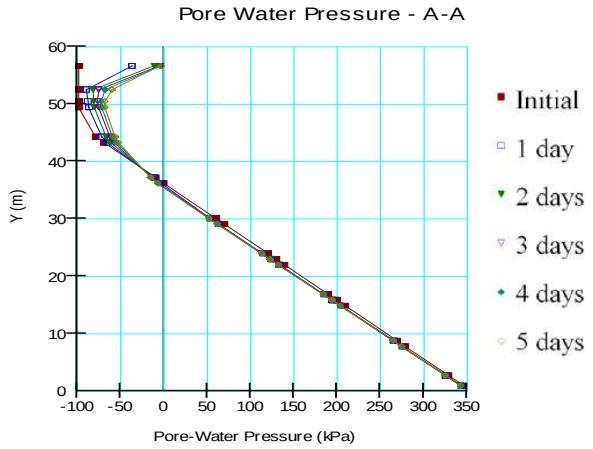

Figure 20: Pore water distribution vs depth in sections 1 for slope with relict joints and with surface drainage improvement (Permeability of vegetation layer = 10^{-7} m/s)

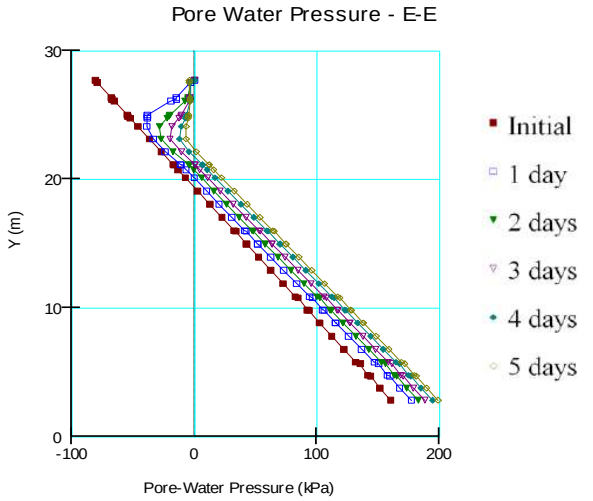

Figure 21: Pore water distribution vs depth in sections 2 for slope with relict joints and with surface drainage improvement (Permeability of vegetation layer = 10^{-7} m/s)

7.4 Slope Stability Analysis

An analysis of the stability of the slope at the end of each day was done using SLOPE/W software after incorporating the pore water pressure distributions obtained from the seepage analysis.

Direct shear tests performed on undisturbed samples obtained from a location behind the scar, initially after full saturation and subsequently at different levels of saturation while measuring the matric suction (Vasanthan 2016). The saturated shear strength parameters are presented in Table 2. Parameters of filling material in relict joints deduced based on the experiences on similar soils are presented in Table 3. A ϕ^b value of 33° was used based on the studies done by Vasanthan (2016).

Table 2: Shear strength parameters of the soil profile

Soil type	Unit Weight (γ_{eff})	Effective Cohesion (c′)	Friction angle (ϕ′)
Sandy Silt	19 kN/m³	10 kPa	33 °

Table 3: Shear strength parameters of the filling material in relict joints

Filing material	Unit Weight (γ_{eff})	Effective Cohesion (c′)	Friction angle (ϕ′)
Loose fill	12 kN/m³	2 kPa	15 °

Analyses were done using the GEOSLOPE SLOPEW (2007) software with the Spencer's method considering circular shaped slope failures through the grid and radius approach as it yielded kinematically feasible failure surfaces.

The Mohr Coulomb shear strength relationship developed for an unsaturated soil (Fredlund et.al.,1978) was incorporated in SLOPE/W analysis.

$$\tau_f = c' + (\sigma_n - u_a)\tan\phi' + (u_a - u_w)\tan\phi^b \quad \text{Eq [5]}$$

Where, τ_f -shear strength of unsaturated soil; c′ effective cohesion; $(\sigma_n - u_a)$ net normal stress; ϕ′ effective angle of internal friction; $(u_a - u_w)$ matric suction and ϕ^b angle indicating the rate of increase in shear strength relative to the matric suction.

The factor of safety (F) is defined as;

$$F = \frac{\tau_f}{\tau_m} \quad \text{Eq [6]}$$

7.4.1 Results of slope stability analysis

The variations in the pore pressure regime obtained under different conditions in the parametric analysis were incorporated in the stability analysis and the variation of factor of safety as the rainfall prolonged is graphically presented in Figure 22.

The results in Figure 21 and Figure 22(a) indicate that if there are no relict joints and the drainage measures are completely intact and are functioning as designed the FOS is greater than unity on the day and failure would not have occurred. Even if the relict joints are present the factor of safety will be greater than unity if the drainage system is properly functioning Figure 21 and Figure 22(b).

Even if the surface drainage system is not effective, if there were no relict joints the factor of safety would be

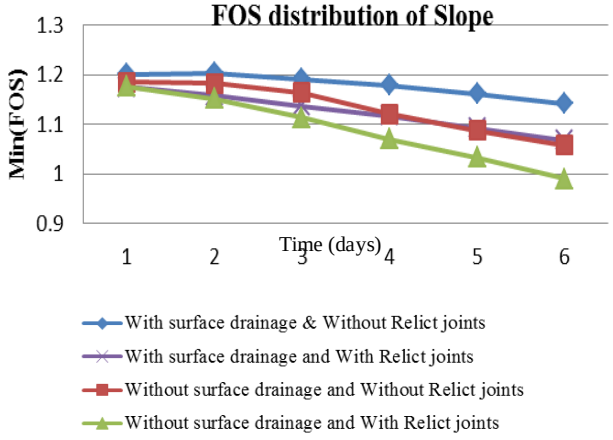

Figure 22: FOS distribution without surface drainage

The corresponding critical failure surfaces at the day of failure are presented in Figure 23.

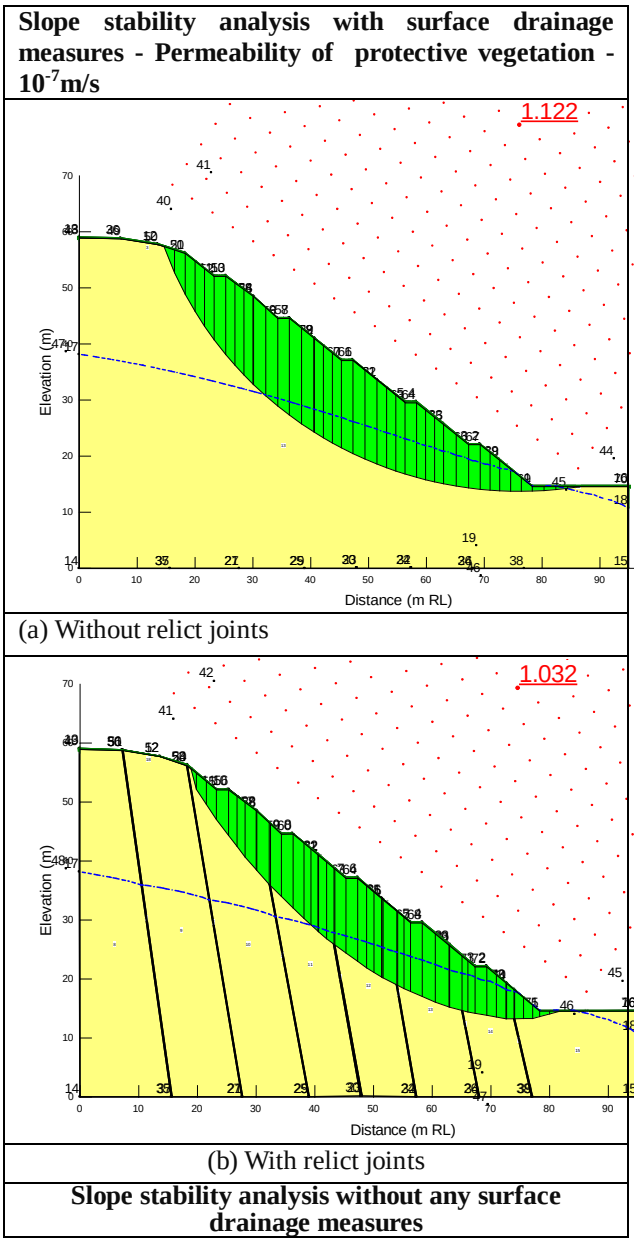

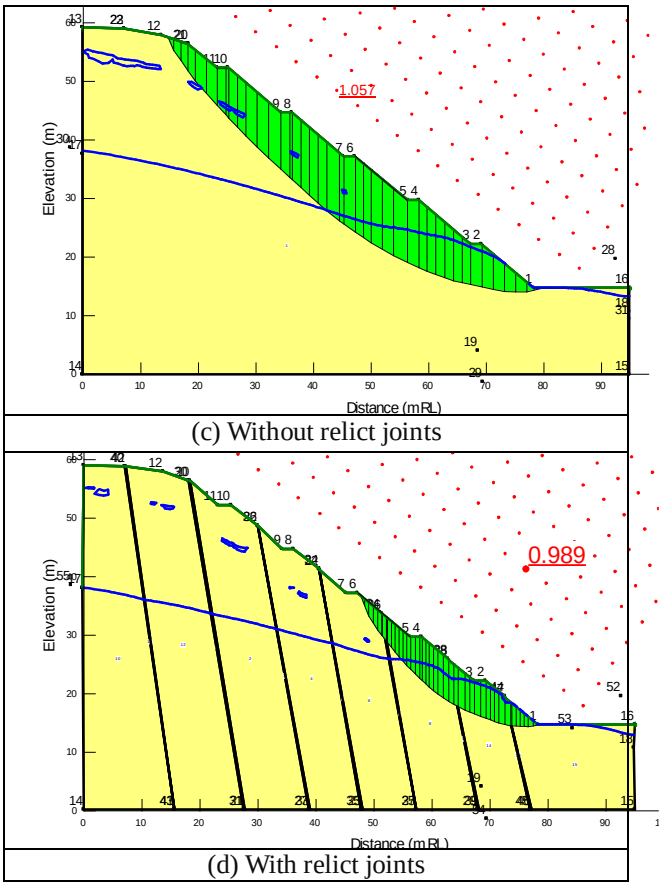

Figure 23: Results of Slope Stability analysis using pore water pressure results from SEEP\W at the failure day

slightly greater than unity (Figure 21 and Figure 22(c)).If there are relict joints and the surface drainage system is not effective the FOS would be lower than unity on that day and would indicate failure (Figure 21 and Figure 22(d)). The critical failure surface corresponding to this situation is quite close to the actual failure. Actual failure occurred at a height of around 20 m damaging berm drains at three levels and cascade drains and the failure surface was quite shallow. The predicted failure surface was also quite shallow and started from a height of 22m damaging berm drains at three levels.

8. CONCLUSIONS

A back analysis was done on the slope failure that took place at Welipenna in the Southern Expressway. The slope was formed of a Sandy Silt which was the product of the insitu weathering of the parent metamorphic rock. The presence of relict joints were evident and incorporated into the analysis. The boudinage structures encountered in the rectification work were not included in the analysis. There were some indications on the defects in the surface drainage system. The antecedent matric suction/pore pressure distribution at the triggering rainfall event was also not known. As such, the back analysis had to be performed in the form of a parametric study. The characteristics such as;

Permeability function, SWCC and shear strength parameters of the unsaturated soils present in the site were experimentally determined and incorporated into the analysis.

The parametric analysis was done for the cases; With and without a proper surface drainage system. Analyses were done for both the presence of relict joints and the absence of relict joints. Relict joint were considered to be filled with a loose material. The antecedent matric suction was given an upper value of 100 kN/m^2.

The results of the analysis revealed the diminishing of the matric suction, development of perched water table and rise of ground water table as rainfall prolongs. The rise of ground water table at the toe of the slope was quite dominant. These destructive effects were greater when the relict joints are present and when the surface drainage system is not effective. The factor of safety on the day of failure reached a value less than unity when the relict joints are present and there are defects in the surface drainage system.

This highlights the importance of close monitoring of the surface drainage systems installed and paying prompt attention to any maintenance requirements. The modeling of infiltration process under different conditions revealed that the rise of ground water table is quite significant at the toe of the wall. Therefore when natural slopes are excavated into steeper profiles for construction of highways it is recommended to have a series of sub horizontal drains at the toe level even if the ground water table is found to be lower than the toe level in general.

REFERENCES

1. Dharmasena, U.K.N.P., Bandara, K.N and Kulathilaka, S.A.S.,(2015) , "Back Analysis and Rectification of a Failed Cut Slope in the Southern Expressway", ICGE-Colombo-2015 Organized by SLGS, Colombo, Sri Lanka. pp 543-546
2. Fredlund, D. G. and Rahardjo, H., (1993), "Soil mechanics for unsaturated soils". New York: Wiley.
3. Fredlund, D.G., Morgenstern, N.R and Widger R.A, (1978) "The shear strength of unsaturated soils." Canadian geotechnical journal, 15, pp. 313-321
4. Landslide Research and Risk Management Division, NBRO, " Proposal for rectification of failed slope at Ch 42+340 to Ch 42+400 in STDP", 2013
5. Sujeevan.V , and Kulathilaka .S.A.S, Rainfall Infiltration Analysis in Unsaturated Residual Soil slopes, Paper published in the Geotechnical Journal, Journal of the Sri Lankan Geotechnical Society, Vol 6 -December 2011-pp9-19
6. Vasanthan, N., (2016), "Establishment of fundamental characteristics of some unsaturated Sri Lankan residual soils", Thesis submitted in partial fulfillment of the requirements for the degree of Master in Engineering, University of Moratuwa.
7. GEO-SLOPE International Ltd, Second Edition, May 2007 "Stability Modeling with SLOPE/W 2007" An Engineering Methodology Calgary, Alberta, Canada.
8. GEO-SLOPE International Ltd, Second Edition, May 2007 "Seepage Modeling with SEEP/W 2007" An Engineering Methodology Calgary, Alberta, Canada.

A laboratory-scale numerical study of CO_2 flow through coal under down-hole stress conditions: Application to CO_2 storage

Ranathunga A.S [1], Perera M.S.A.[2] and Ranjith P.G. [3]

1 *Lecturer, Department of Civil Engineering, University of Moratuwa, Sri Lanka*
2 *Lecturer, Department of Infrastructure Engineering, The University of Melbourne, Australia*
3 *Professor, and Director, Deep Earth Energy Laboratory, Monash University Australia*

ABSTRACT: Existing studies highlight the uncertainty in the process of CO_2 sequestration in deep coal seams, mainly due to the associated CO_2 adsorption-induced coal matrix rearrangements. Therefore, it is important to investigate how the CO2 flow varies through the coal seam and the related effect on CO_2 storage capacity. Several experimental studies have been conducted on this, however, the inability to represent deep coal seam conditions in laboratory experiments is one of the main drawbacks in relating experimental results to field conditions. The main objective of this study is therefore to determine the permeability behaviour in coal for CO_2 flow and the corresponding CO_2 storage capacity using a laboratory-scale numerical model of deep coal seams. A macro-scale (203 mm diameter and 1000 mm long) model was developed using COMSOL Multiphysics software to represent a thin coal seam, and the model was successfully calibrated and validated using the data obtained using the experimental results of reconstituted brown coal specimens by Ranathunga et al. (Fuel, 158:864-873, 2015) and Ranathunga et al. (Geomechanics and Geophysics for Geo-Energy and Geo-Resources, 3:13-28, 2016). The model was then extended to predict the flow characteristics such as permeability, CO_2 pressure and CO_2 concentration distributions, and CO_2 storage capacity in coal under higher injection pressures and deeper reservoir depths. According to the model results, CO_2 permeability through the coal mass is negatively affected by both CO_2 pressure and the depth of the coal seam, whereas this effect is decreased at higher depths and CO_2 pressures. Further, the flow parameters, such as CO_2 pressure and CO_2 concentration, reduce along the sample length with increasing depth. The model can accurately predict the experimental observations of CO_2 storage capacities, which showed an increase in CO_2 storage over time. However, for a given depth, CO_2 concentration increases with increasing injection pressure. In spite of the lower pressure developments and permeability existing under higher effective stresses, greater amounts of CO_2 can be sequestrated into coal seams if sufficient time is allowed for CO_2 permeation.

Key Words*: CO_2 storage; Core flooding test; Effective stress; Laboratory-scale mode*

1. INTRODUCTION

The injection of CO_2 into deep coal seams causes their chemical and physical properties to change greatly, which causes the amount of injectable CO_2 into and producible CH_4 from these seams to become unpredictable. Much research has been conducted on the effects of CO_2 injection on coal and has revealed that there is a great degree of swelling caused by CO_2 adsorption that, in turn, can cause the permeability of the coal mass to be severely Reduced (Anggara et al., 2013; Day et al., 2008; Perera et al., 2011; Ranathunga et al., 2015). In these research studies, De Silva and Ranjith (2013), Ranathunga et al. (2015) and Ranathunga et al. (2016) conducted several macro-scale studies using reconstituted low rank brown coal samples to study the effect of CO_2 and reservoir properties on the CO_2 flow behaviour in coal using reconstituted coal samples to minimise the effect of heterogeneity. The macro-scale tests provide a better location-dependent representation of the CO_2 adsorption-induced coal structure modification and have the ability to capture the changes in CO_2 storage capacity along the coal mass, offering a good correlation of measured data with field conditions.

However, these studies were conducted under limited test conditions, due to the extensive time required to conduct such macro-scale tests. Therefore, an effort was made in this study to model the experimental observations using the COMSOL Multiphysics simulator. The results were then extended to simulations using COMSOL Multiphysics, particularly on the impact of CO_2 properties (phase and pressure) on CO_2 sequestration and its influence on CO_2 storage for macro-scale experimental conditions. These have not been studied to date using numerical modelling. For the proposed numerical model, the experimental results obtained by Ranathunga et al. (2015) based on core-flooding tests conducted under different CO_2 phase and pressure conditions were used and the results were validated using the experimental results obtained by Ranathunga et al. (2016). The validated model was then extended to higher axial stresses and CO_2 pressures to represent the situation of potential

deep coal seams, which are preferable for CO_2 sequestration. The model effectively represents the field conditions, confirming the reliability of the modelling approach used.

2. MODEL DEVELOPMENT

This section presents the methodology adopted to develop the numerical model using COMSOL. A two-dimensional finite element model to simulate the core-flooding tests performed under different CO_2 saturation conditions was developed using COMSOL Multiphysics using the *Poroelasticity* interface in the Structural Mechanics module and the *Transport of diluted species in porous media* interface in the Chemical Species Transport module.

2.1 Theory used for model development

2.1.1 Structural mechanics: Poroelasticity

Generally, the poroelastic model describes the linked interactions between fluid and deformation in porous media. This module assumes the domain of the material consists of both the porous matrix and the fluid filling the pore (solutes), and both carry loads. The formulation used for structural analysis in COMSOL for both small and finite deformations is totally Lagrangian. The displacement is considered as a function of the material coordinates (X, Y, Z) in the total Lagrangian configuration, and hence the total strain tensor is written in terms of the displacement gradient (∇u) (see Eq. [1]).

$$\nabla u = \begin{bmatrix} \frac{\partial u}{\partial X} & \frac{\partial u}{\partial Y} & \frac{\partial u}{\partial Z} \\ \frac{\partial v}{\partial X} & \frac{\partial v}{\partial Y} & \frac{\partial v}{\partial Z} \\ \frac{\partial w}{\partial X} & \frac{\partial w}{\partial Y} & \frac{\partial w}{\partial Z} \end{bmatrix} \quad \text{Eq [1]}$$

The physical components of the radial and axial displacement, *u* and *w*, are used as independent variables for the axially symmetric geometry. Therefore, the Green-Lagrange strain tensor (ε) can be defined as in Eq. [2].

$$\varepsilon = \frac{1}{2}[\nabla u + (\nabla u)^T + (\nabla u)^T \nabla u] \quad \text{Eq [2]}$$

An elastoplastic model was assumed for the numerical study. Here, the structural mechanics equation from the solid mechanics module is modified to incorporate the fluid pressure gradient, and hence an additional term $\alpha_\beta\, p_f\, I$, is inserted as the fluid to the structure coupling term. This coupling term links the structural deformation to fluid flow, and consequently the stress, strain and the pore pressure of linear poroelastic material are related with the following equation (Eq. [3]):

$$S - S_0 = C:(\varepsilon - \varepsilon_0 - \varepsilon_{intel}) - \alpha_\beta \rho_f I \quad \text{Eq [3]}$$

where, S and ε are stress and strain tensor, S_0 and ε_0 are the initial stress and strain, ε_{inel} is the sum of all inelastic strains, C is the 4th order elasticity tensor, α_B is the Biot Willis coefficient and p_f is the fluid pore pressure.

2.1.2 Structural mechanics: Darcy's law

Darcy law can be used to model the fluid flow in a porous medium, where the major driving force is the pressure difference. Darcy's equation in the subsurface flow module is modified to include the additional term, the time rate change of volumetric strain ($(\partial_{evol})/\partial t$) to link fluid flow with structural deflection, as shown in Eq. [4]

$$p_f S \frac{\partial p_f}{\partial t} + \nabla.\rho\left[-\frac{k}{\mu}\nabla p_f\right] = Q_m - p_f \alpha_B \frac{\partial e_{vol}}{\partial t} \quad \text{Eq [4]}$$

where, $(\partial_{evol})/\partial t$ is the rate of change in volumetric strain derived from solid displacement, Q_m is the mass source term, ρ is fluid density, S is the storage coefficient, k is the permeability of the porous medium and μ is the dynamic viscosity of the fluid. Here, the storage coefficient S is calculated by Eq. [5].

$$S = \frac{\varepsilon_p}{K_f} + (\alpha_B - \theta)\left(\frac{1-\alpha_B}{K_d}\right) \quad \text{Eq [5]}$$

where, ε_p is the porosity of the material, K_f is the bulk modulus of fluid (inverse of fluid compressibility), K_d is the drained bulk modulus ($K_d=(1-\varepsilon_p)\,K_S$), and Ks is the bulk modulus of the material).).

2.1.3Transport of diluted species in porous media

The transport of diluted species in porous media interface was used to model the CO_2 concentration in the brown coal sample, and this interface was coupled with the Darcy law interface using Darcy velocity (*u*) in Eq. [6].

$$\frac{\partial}{\partial t}(\theta c_i) + \frac{\partial}{\partial t}(\rho_b c_{p,i}) + \frac{\partial}{\partial t}(\alpha_v c_{G,i}) + u.\nabla c_i = \nabla.\left[(D_{D,j} + D_{e,j}).\nabla c_i\right] + R_i + S_i \quad \text{Eq [6]}$$

where, θ is liquid volume fraction, c_i is the concentratıon of species, ρ_b is the bulk density, $c_{(P,i)}$ is the amount adsorbed to the solid particles, α_v is the resulting gas volume fraction (ε_p-θ), $c_{(G,i)}$ is concentration of species in the gas phase, $D_{(D,j)}$ is the dispersion tensor, $D_{(e,j)}$ is the diffusion tensor, u is the directional velocity, R_i is the reaction rate expression, and S_i is an arbitrary term. In this model, CO_2 adsorption into the coal mass was modelled by the Langmuir equation and this is shown in Eq. [7]

$$.c_{P,i} = \frac{V_L p}{(p+P_L)} \quad \text{Eq [7]}$$

where, V_L and P_L are Langmuir volume and pressure coefficients respectively.

To numerically represent the coal's hydro-mechanical behaviour during CO_2 sequestration, the above mentioned modules: Structural mechanics and Transport of diluted species in porous media were coupled before running the model in COMSOL.

3. MODEL VALIDATION USING EXPERIMENTAL DATA

The numerical study is based on the results of a previous experimental study conducted on CO_2 flow variation in reconstituted Victorian brown coal under different CO_2 phase and pressures by Ranathunga et al. (2015) and Ranathunga et al. (2016). Here, reconstituted brown coal samples results were used to avoid the complexities related to the heterogeneity of coal. In the previous studies, sub-critical (6 and 7 MPa) and super-critical (8, 9 and10 MPa) CO_2 were permeated in reconstituted brown coal samples 203 mm in diameter and 1000 mm in length at 38 ^{0}C (>31.8 ^{0}C is the critical temperature of CO_2). The material properties for the modelling were obtained from the experimental results and are further discussed in the following sections.

4. BASIC ASSUMPTIONS

1. Brown coal is a linear poroelastic isotropic material, and Poro elasticity theory can be used to model the linked interaction between the flow and solid deformation.
2. The major fluid driving force across the coal specimen is the pressure gradient, and hence Darcy's law is valid.
3. The adsorption of CO_2 into the coal matrix can be modelled using Langmuir isotherms.
4. CO_2 flow through the coal specimen is due to advection, diffusion and dispersion, and sorption.
5. No moisture or other gasses were present in the coal sample before CO_2 permeation.

5. MODEL DEFINITION AND BOUNDARY CONDITIONS

To simulate the experimental conditions, a 2-D model was first developed for a width of 1000 mm (the length of the tested coal specimen) and a height of 203 mm (the diameter of the tested coal specimen), which was then converted into a 3-D model using the Model builder interface in the COMSOL Multi physics simulator. The boundary conditions adopted for the structural mechanics module (mechanical boundary conditions) are as follows:
Under laboratory condition, the circumference and the left-side base of the sample consist of a fixed pressure cell casing and hence are assumed to be a fixed boundary. The right side of the sample moves inward and outward from the cell to compress the sample and hence the axial load (F_a) was applied to the right-side base of the sample. CO_2 was injected from the right-side base of the sample and was introduced as an *Inflow flux*. The circumference of the sample (top and bottom boundaries) has no flow boundaries. When considering the downstream of the sample, the experiments were conducted under undrained conditions, and the pressure development of a fixed volume at the downstream was observed to calculate the pressure gradients along the coal specimen. Further, there was no outflow from the downstream during the gas injection. An 8 mm long area was introduced to the left side of the model to represent the fixed downstream volume (32.36 cm^3) with a 100% initial porosity (empty volume). The initial permeability of the downstream volume was selected as 1000 mD (>>> brown coal initial permeability, to better represent the initial void volume there) and the end boundary of the downstream volume was set as fixed with a no-flow boundary (Perera et al., 2012). Parametric sweeps were used in the model for CO_2 injection and axial loads, and injection pressures of 5-20 MPa and axial loads of 0-15 MPa were applied to the sample. The overall details of the geometry and boundary conditions adopted for the model are shown in Figure 1

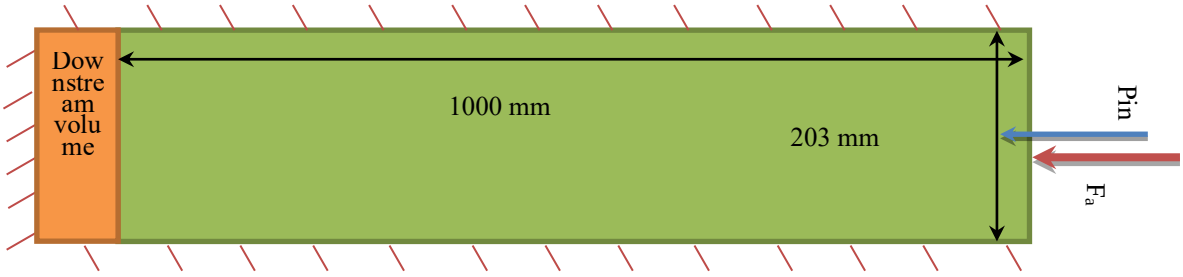

Figure 1: Dimensions, boundary conditions, and boundary load for the macro-scale COMSOL model

6. MODEL INPUT PARAMETERS

The thermodynamic properties, such as density, viscosity and adiabatic compressibility of CO_2, vary with the fluid pressure for a given temperature. The relationships between the thermodynamic properties and mean CO_2 pressure within the sample (*Pm*) (the temperature was kept constant throughout the experiments) were derived using the REFPROP database(McLinden et al., 1998), and these formulations were entered into COMSOL (see Eqs. [8 - 10]). Further, the CO_2 concentration of the sample was obtained from Eq. [12] using the COMSOL model parameter for Darcy's velocity field *X* component. The material properties for the model were obtained from the experimental results. The input parameters for the model are shown in Table 1.

Density of CO_2 ($\rho_{CO2} - kgm^{-3}$):

$$\rho_{CO2,sub} = 15.216 \exp(4E-07P_m)$$

R^2 = 0.9789 for $P_m \leq$ 7.38 MPa Eq [8a]

$$\rho_{CO2,super} = -1E-12P_m^2 + 6E-05P_m + 266.85$$

R^2 = 0.9886 for $P_m >$ 7.38 MPa Eq [8b]

Dynamic viscosity of CO_2 ($\mu_{CO2} - MPa.s$):

$$\mu_{CO2,sub} = 5E-19P_m^2 - 3E-12P_{in} + 2E-05$$

R^2 = 0.9987 for $P_m \leq$7.38 MPa Eq [9a]

$$\mu_{CO2,super} = 6E-09P_m^{0.5689}$$

R^2 = 0.9757 for $P_m >$ 7.38 MPa Eq [9b]

Adiabatic compressibility of CO_2 (β_{CO2}-1/MPa):

$$\beta_{CO2,sub} = 2.5416\ P_m^{-1.081}$$

R^2 = 0.9867 for $P_m \leq$ 7.38 MPa Eq [10a]

$$\beta_{CO2,super} = 149609P_m^{-1.866}$$

R^2 = 0.9810 for $P_m >$ 7.38 MPa Eq [10b]

where, $P_m = \frac{P_{in}+P_{out}}{2}$,

where P_m is mean CO_2 pressure through the sample, P_{in} is the CO2 injection pressure (or upstream pressure) and P_{out} is the downstream pressure developed at the downstream volume (when the pressure developments of the downstream achieve the steady state). P_{out} varies with the injection pressure and the axial load applied on the sample and Eq. [12] was developed to obtain downstream pressure at steady state using the experimental data from Ranathunga et al. (2015) and Ranathunga et al. (2016).

$$P_{out} = -0.0527F_a + 0.7839P_{in} - 2.2347 \quad \text{Eq [11]}$$

Concentration of CO_2:

$$c = \frac{[poro.uf \times \rho_{CO2}]}{0.04401}\ [mol/(m^2 s)] \quad \text{Eq [12]}$$

where, $poro.uf$ is the Darcy's velocity field *X* component obtained from the model.

The CO_2 flow rate (Q, steady state) and the permeability (k) of coal specimen are given by Eqs. [13] and [14].

$$Q = -1.4602 \times 10^{-11}F_a - 8.651794 \times 10^{-13}P_{in} + 0.00028\ [l/h] \quad \text{Eq [13]}$$

$$\frac{2QP_{out}(\mu_{CO2,i})L}{A(P_{in}^2 - P_{out}^2)}\ [m^2] \quad \text{Eq [14]}$$

where, μ_(CO_2,i) is the dynamic viscosity of the CO_2 present in the sample and i = sub- and super-critical CO_2 phases (refer to Eqs. [9a,b]). It should be noted that only the steady-state flow rate values for 6, 8 and 10 MPa CO_2 injection pressures under 11 and 17 MPa axial stresses were used to develop the empirical relationship shown in Eq. [13], and the rest of the data were used to validate the model. Finally, the model was extended to higher axial loads and CO_2 injection pressures to obtain the effect of CO_2 properties and in situ stresses on the brown coal sample.

Table 1: The input parameters for the model

Model Parameter	Value
Coal sample properties	
Sample diameter (D)	203 mm
Sample length (L)	1000 mm
Density (ρ)	1097.8 kg/m^3
Young's modulus (E)	72.01 MPa (Jasinge, 2010)
Poisson's ratio (ϑ)	0.27 (Jasinge, 2010)
Porosity (ε_p)	0.41 (Jasinge, 2010)
Biots-Willis coefficient (α_B)	0.9 (Perera et al., 2013)
Pore volume compressibility (c_p)	2.96E-05 1/Pa (De Silva and Ranjith, 2014)
Matrix shrinkage/swelling compressibility (c_m)	1.21E-05 1/Pa (De Silva and Ranjith, 2014)
Langmuir volume for CO_2 adsorption for brown coal (V_L)	29.11 m^3/kg (Jasinge, 2010)
Langmuir pressure for CO_2 adsorption for brown coal (P_L)	0.578 MPa (Jasinge, 2010)
Downstream properties (explained in Section 4)	
Downstream length (L_{ds})	8 mm
Porosity (ε_{ds})	1
Initial permeability ($k_{o,ds}$)	1000 mD (Perera et al., 2012)
CO_2 properties (explained in Section 4)	
Density (ρ_{CO2})	Refer Eqs. [8a,b]
Dynamic viscosity (μ_{CO2})	Refer Eqs. [9a,b]
Adiabatic compressibility (β_{co2})	Refer Eqs. [10a,b]
Initial CO_2 concentration (c_o)	0 kg/m^3
CO_2 concentration (c)	Refer Eq. [12]
Boundary conditions (parametric sweep)	
Axial load (F_a)	5 - 20 MPa
CO_2 injection pressures (P_{in})	0 - 15 MPa

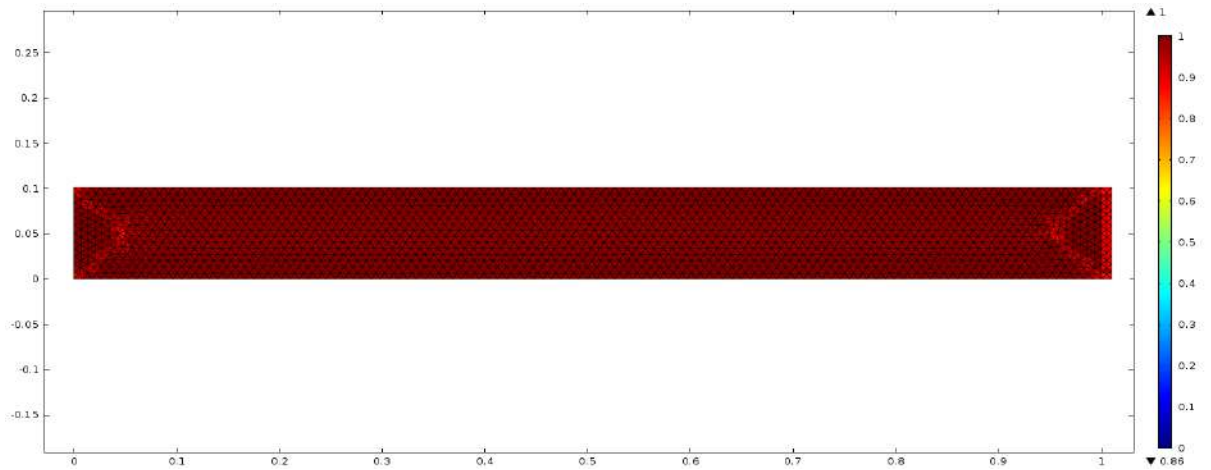

Figure 2: Mesh quality plot for the mesh pattern used in the model

7. MESHING AND ELEMENT SIZES

A 2-D mapped meshing was assumed for the model since it consists of a simple rectangular geometry bounded by four boundary segments with no holes. By defining the number of elements at each side, a mapped mesh was introduced to the model. The meshing parameters are shown in Table 2 and the assumed mapped mesh and mesh quality plot are shown in Figure 2. The colour range 0 means poor quality and 1 means good quality in Figure 2, which indicates the assumed mesh pattern fits the geometry well.

Table 2: Mesh parameters

Property	Value
Number of degrees of freedom	23526
Number of elements (triangle)	158118
Number of boundary elements	1763

8. MODEL RESULTS AND DISCUSSION

8.1. Effect of CO_2 injection pressure on coal mass permeability

A comparison of the coal mass permeability values obtained from the experiments and the COMSOL model for 11 and 17 MPa axial loads is shown in Figure 3. According to the figure, the model-predicted permeability values are in good agreement with the experimental results. Particularly for higher CO_2 pressures (12 and 14 MPa were not used for the empirical relation-ship developments), the model-predicted permeability values show only around 7 to 9 % errors compared with the experimental results (see Table 3). Next, the model was extended to calculate the CO_2 permeability of brown coal under higher injection pressures, which could not be found under laboratory conditions. The results are shown in Figure 4.

Table 3:Error between experimental and model predicted permeability values

Axial load (MPa)	CO_2 injection pressure (MPa)	Error (%)
11	7	6.12
	9	4.07
17	7	1.54
	9	4.97
	12	7.47
	14	8.94

According to Figure 4, the expected permeability reduction with CO_2 adsorption is continued at both lower (< 6 MPa) and higher (> 14 MPa) injection pressures. As observed by Ranathunga et al. (2015) and Ranathunga et al., (2016), the permeability reduction is increased under higher CO_2 pressures than lower pressures. For ex-ample, a 5 to 6 MPa sub-critical CO_2 pressure increase causes a permeability reduction of 9.15%, while the reduction for 15 to 16 MPa CO_2 pressure increment is around 54.7%.

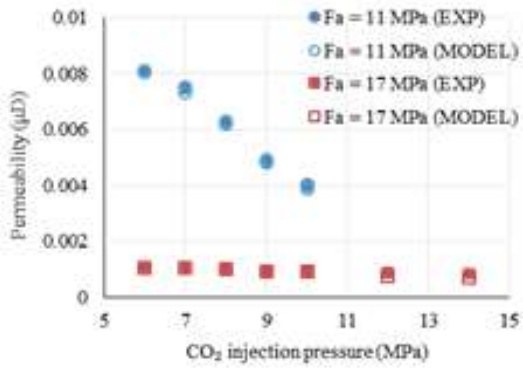

Figure 3: Comparison of permeability values obtained from experiments (solid points) (Ranathunga et al., 2015; Ranathunga et al., 2016) and COMSOL model (hollow points) for 11 and 17 MPa axial loads

Therefore, permeability reduction is in-creased by around 6- fold when the upstream pressure is raised by 10 MPa. As explained previously, the greater adsorption potential under higher CO_2 pressures reduces the flow through the coal sample, resulting in greater permeability reductions under higher CO_2 pressures com-pared to lower pressures.

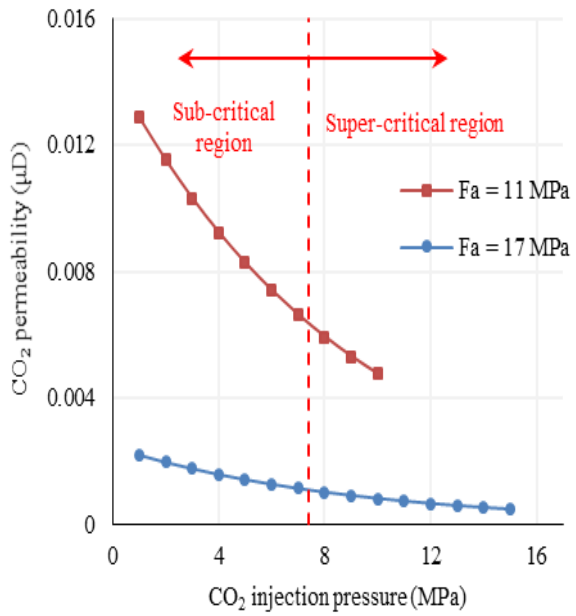

Figure 4: CO_2 permeability for further sub- and super-critical CO_2 flows under 11 and 17 MPa axial loads

It would be interesting to investigate whether this flow behaviour continues in deeper coal seams. This was studied next by extending the model to higher axial loads representing different depths.

8.2. Effect of reservoir depth on coal mass permeability

Figure 5 shows the CO_2 flow variation at different reservoir depths obtained from the extended laboratory-scale COMSOL model. As observed by Ranathunga et al. (2016), the CO_2 flow ability along the coal mass is reduced at greater depths due to the higher effective stress. For example, during 6 MPa sub-critical CO_2 flow, around 65.9% and 54.7% reduction of CO_2 flow was observed when the depth was increased from 0.4 to 0.5 km and 0.5 to 0.6 km, respectively (see Figure 5). This flow reduction is less at greater depths than lower depths. Similar results were observed by Ranathunga et al. (2017), who observed around 69% and 56% reduction of CO_2 permeability when the depth was increased by similar values (from 0.4 to 0.5 km and 0.5 to 0.6 km respectively) for low rank coal, based on tri-axial experiments. Hence, these findings from the COMSOL model con-firm the lesser influence of seam depth on CO_2 flow reduction.

In addition, when the coal seam depth is in-creased from 0.8 to 0.9 km, the CO_2 permeability is reduced by 78.4% for 4 MPa sub-critical CO_2 injection, while there is around a 53.5% reduction for 14 MPa super-critical CO_2 injection (refer to Figure 5). Similar behaviour was observed by Ranathunga et al. (2017) in meso scale flow studies on brown coal, which obtained around 80% and 75% flow reduction for 6 MPa (sub-critical) and 9 MPa (super-critical) CO_2 injections when the confining pressure in-creased from 11 to 14 MPa (approximately 0.4 to 0.5 km). Under higher effective stresses, the CO_2 permeability through the coal mass is reduced and hence the expected flow reductions under higher CO_2 pressures (super-critical CO_2) are also lower. Therefore, the experimental findings of greater CO2 flow reduction under higher effective stresses which gradually decrease

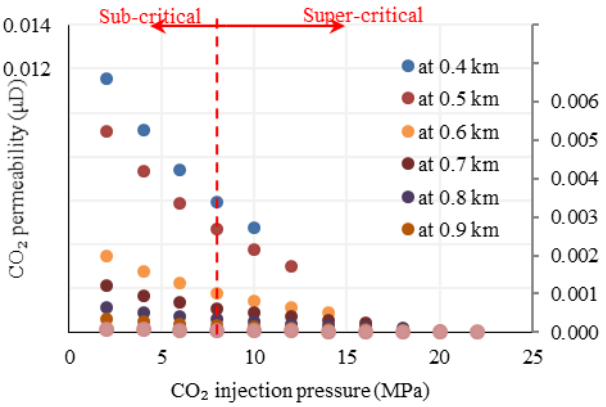

Figure 5: CO_2 permeability variation at greater depths

with increasing depth and injection pressure are further confirmed by the model results. This implies that the influence of CO_2 phase is more dominant in shallow coals seams than deep seams, which is preferable for CO_2 storage, as it is often carried out at deep depths.

8.3 CO_2 pressure and concentration distribution along the coal sample

8.3.1 CO_2 pressure distribution along the coal specimen

The steady-state flow under experimental conditions at 6 MPa injection and 17 MPa axial load was obtained after around 18 hours of CO_2 injection (Ranathunga et al., 2016). The CO_2 pressure distribution in brown coal up to 18 hours of CO_2 injection (steady-state time under experimental conditions) at 6 MPa injection pressure and 17 MPa axial load is shown in Figure 6. According to the figure, CO_2 moves gradually with time due to the pressure difference (advection) and reaches the steady-state condition. As there is a greater pressure difference between the upstream (Pin) and downstream boundaries, CO_2 movement through brown coal is mainly governed by the pressure-driven advection process (Darcy's flow). Under the steady-state condition, the CO_2 pressure at the right boundary is equal to the injection pressure (Pin) and the left boundary is at steady-state downstream pressure (P_{out}).

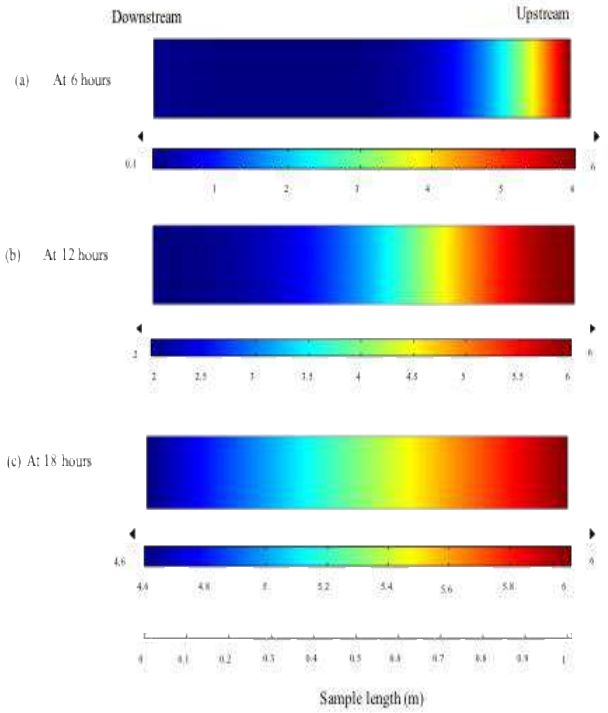

Figure 6: CO_2 pressure distribution (in MPa) in brown coal after 6, 12, and 18 hours of 6 MPa CO_2 injection under 17 MPa axial load

the CO_2 pressures through the brown coal specimen after 24 hours (assuming 24 hours is sufficient time to achieve the steady-state condition for all the injection pressures) were plotted for 6 and 8 MPa CO_2 injections for 11 MPa axial stress and compared with the experimental results

observed for the respective conditions (refer to Figure 7). According to the figure, there is good agreement between the experimental pre-dictions of pressure development along the coal specimen and the model-predicted data. The pressure distribution along the sample is almost constant up to around 1/3 of the sample length from the injection point and is gradually reduced up to downstream.

Figure 8 displays the model-predicted pressure development of the coal sample at 6 and 8 MPa CO_2 under different axial stresses. As observed in Figure 7, the CO_2 pressure reduces gradually along the length of the sample for any injection and axial load conditions.

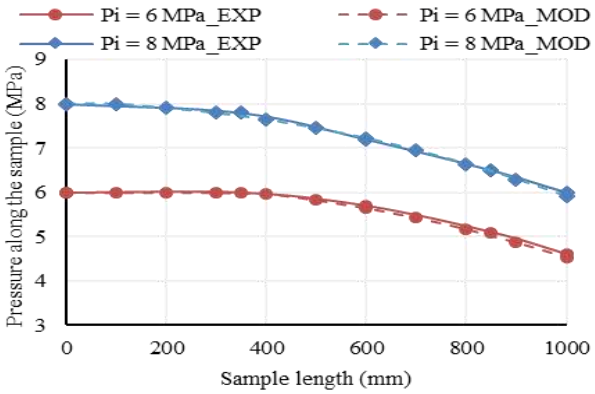

Figure 7: Pressure distribution along the coal sample under 11 MPa axial stress for 6 and 8 MPa CO_2 injections from flow experiments (Ranathunga et al., 2015) and model prediction after 24 hours

For a given injection pressure, the CO_2 pressure decreases with the increase in axial load (depth) after around 1/3 of the sample length at any distance from the injection surface (Figure 8). This may be due to the reduction in pore volume with increases in stress. The effective stress (the difference between axial load and mean injection pressure) increases as the depth increases, and an increase in effective stress causes pore volume shrinkage, leading to reduced flow pathways (Ranjith and Perera, 2011). However, as the injection pressure increases, the effect of depth on CO_2 pressure distribution gradually decreases (Figure 8 (b)). This is possibly due to the reduced CO_2 flow during higher injection pressures (super-critical conditions), which creates lower pressure developments across the coal specimen that eventually has less variation with depth (Nasvi et al., 2014). These results are consistent with the CO_2 pressure variations observed by Ranathunga et al. (2017) for similar low rank coal along the sample.

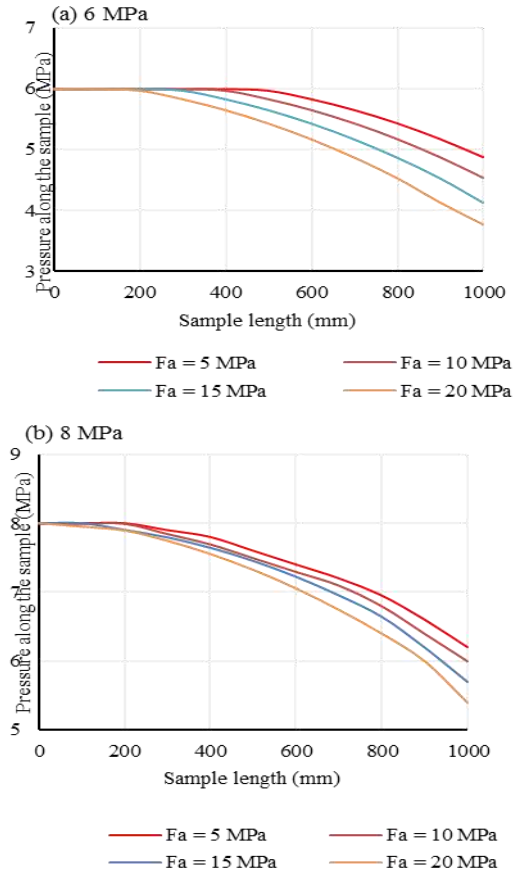

Figure 8: CO_2 pressure development along the brown coal specimen during 6 and 8 MPa CO_2 injection for different axial stresses applied on the sample

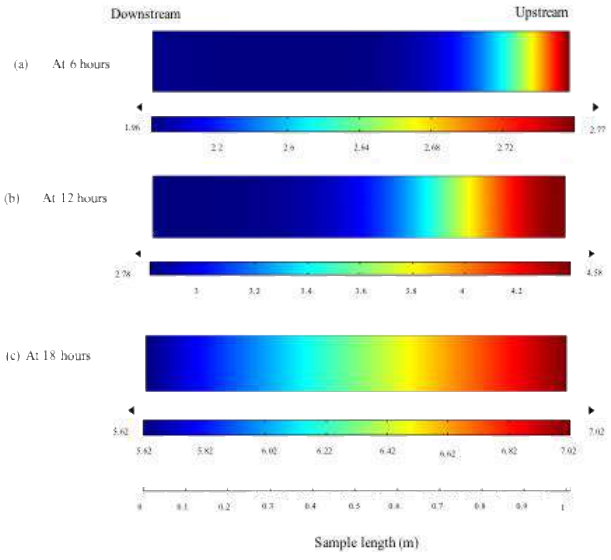

Figure 9: CO_2 concentration (in kg/m^3) distribution in brown coal after 6, 12, and 18 hours of 6 MPa CO_2 injection under 17 MPa axial load

8.3.2 Distribution of CO_2 concentration along the coal specimen during CO_2 permeation

The CO_2 concentration distribution for different injection and axial stresses was studied. The concentration of CO_2 up to 18 hours of CO_2 injection for 6 MPa injection and 17 MPa axial load is shown in Figure 9.

The CO_2 mass spreads with time due to advection and reaches a stable condition after 18 hours of CO_2 permeation. The concentration at the upstream boundary (right-side boundary) of the coal increases from 2.77 to 7.02 kg/m^3 after 6 to 18 hours of CO_2 injection, while the con-centration at the downstream boundary (left-side boundary) increases from 1.96 to 5.62 kg/m^3 during the same time period.

Figure 10 shows the CO_2 concentration distribution in coal after 24 hours of CO_2 injection for different injection and axial loads. In the figure, the CO_2 concentration reduces along the coal sample following a slight exponential behaviour for both 6 and 8 MPa CO_2

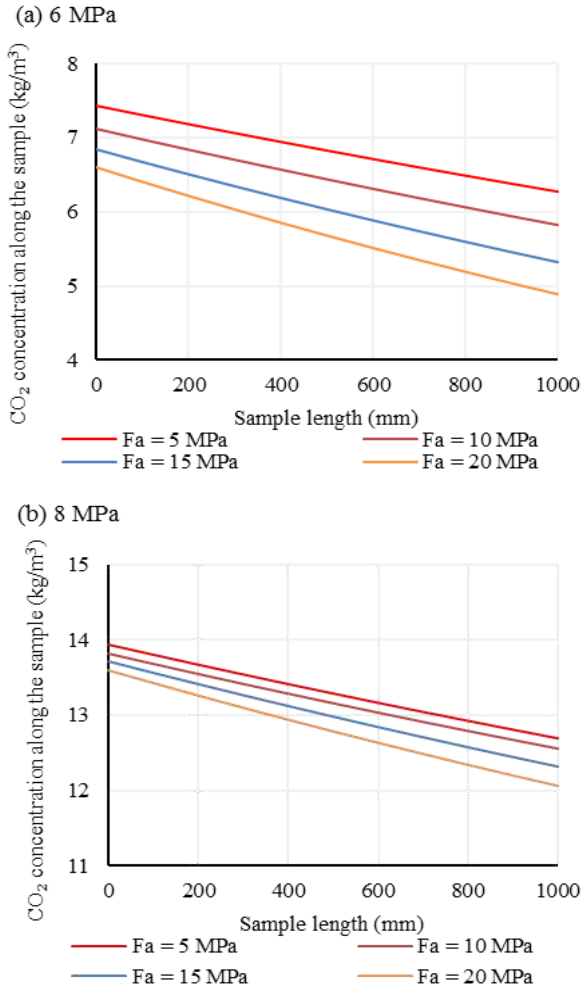

Figure 10: CO_2 concentration along the brown coal specimen during 6 and 8 MPa CO_2 injections for different axial stresses applied on the sample

permeations. As expected, for a given injection pressure, CO_2 con-centration reduces with increases in axial stresses and the results are consistent with the pressure distribution trends obtained for various axial loads. In addition, for a given axial load, CO_2 concentration increases with the increase in injection pressures (Figures 10 (a) and (b)). For example, under 20 MPa axial load, CO_2 con-centration at the upstream (left-side boundary) increases from 6.61 to 13.59 kg/m^3 as the injection pressure is increased from 6 to 8 MPa. This is due to the increase in net CO_2 flux with the increase in CO_2 injection pressure through the coal sample.

As shown in the figure, the experimental observations for the cumulative amount of CO_2 adsorbed into the sample are predicted well by the numerical model for different injection pressures and axial stresses. Further, there is only <8% difference in the experimental and model-

8.4 CO_2 storage capacity of the coal sample

The main purpose of CO_2 sequestration in coal is to store CO_2 stably due to its high adsorption potential to the coal matrix. Therefore, identification of the adsorption potential of a given coal seam is important for the evaluation of the amount of CO_2 that can be stored in the coal mass. According to Ranathunga et al. (2016), a

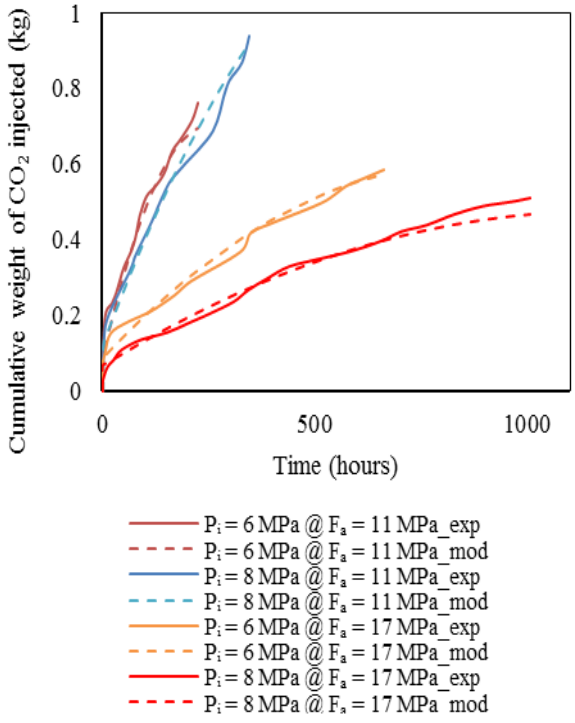

Figure 11: Comparison of model predicted and experimental observations for cumulative CO_2 weight injected into the coal specimen at 6 and 8 MPa CO_2

brown coal specimen showed an increment of cumulative weight of CO_2 injected into the coal sample with time under both 11 and 17 MPa axial stress applications. Assuming that the total amount of CO_2 injected into the coal mass equals the total amount of CO_2 adsorbed into the coal mass(note that the flow tests were conducted under undrained conditions, there-fore the CO_2 injected into the coal sample had no escape paths from the sample during permeation), this observation was compared with the model-predicted cumulative weight of CO_2 adsorbed into the coal mass with time. The results are shown in Figure 11. The amounts of CO_2 adsorbed into the coal specimen under different injection pressures and axial loads were obtained using Eq. [15].

$$W_{ads} = \left(\frac{\rho_{CO_2,i}}{tds.cP_c}\right) AL \qquad \text{Eq [15]}$$

Where, $\rho_{(CO2,i)}$ is the density of CO_2 at a given injection pressure (here $\rho_{(CO2,i)}$ was substituted in mol/m3), i = sub- and super-critical phase conditions (refer to Eqs. [8a,b]), and tds.cP_c is a model parameter for the concentration of species adsorbed into the solid in mol/kg

Predicted total amount of CO_2 adsorbed into the coal mass at the end of 10 days of CO_2 injection (see Table 4). Here, a duration of 10 days means the time after the specimen accomplishes the steady state. Therefore, the total weight of CO_2 that can be adsorbed for various CO_2 pressures under different axial loads after injecting CO_2 for 10 days (after approaching steady-state conditions) was evaluated and the results are shown in Figure 12. According to the figure, the adsorbed CO_2 weight is exponentially reduced

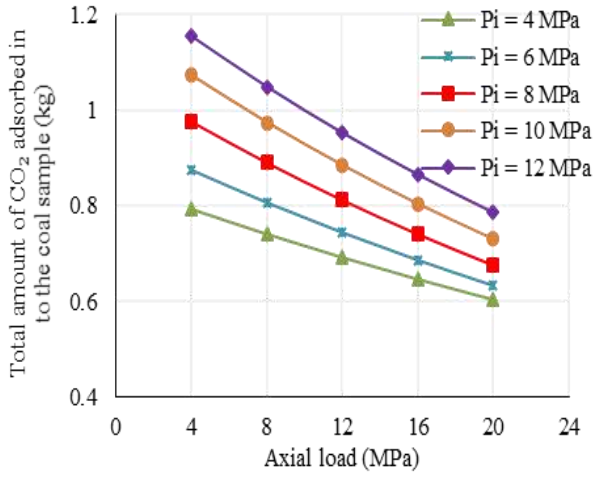

Figure 12: Total amount of CO_2 adsorbed into the coal sample during various CO_2 permeations under different axial loads (10 days after reaching steady-state condition)

With increasing axial loads for a given CO_2 injection pressure. For an example, around 24% and 32% reduction of total CO_2 adsorption was observed for 4 and 12 MPa CO_2 injections when the axial loads are increased from 4 to 20 MPa (refer to Figure 12). This is due to the reduced Adsorption capacity with CO_2 reduced permeability under higher stress applications (Hol et al., 2011). In addition, for a given axial load, the adsorbed CO_2 is also increased. For instance, around 45% in-crease in adsorbed weight is observed for 4 MPa axial load when CO_2 injection pressure is increased from 4 to 12 MPa. As explained by Ranathunga et al. (2), 016the greater adsorption capacity that increases with the injection pressure due to CO_2's inherent physical and chemical properties may increase the adsorbed CO_2 weight. It should be noted that, due to the sufficient time allowed for CO_2 permeation (time to reach steady-state condition plus 10 days), the lower permeability at higher CO_2 pressures are increased. Interestingly, the depth effect is reduced at higher CO_2 pressures, possibly due to the larger number of CO_2 molecules entering the sample at higher pressures leading to greater adsorption into the coal mass

9. CONCLUSIONS

This work focused on the numerical modelling of CO_2 flow through low rank brown coal using the COMSOL Multiphysics numerical simulator for different CO_2 injections and axial loads.

The Photoelasticity interface in the Structural Mechanics module and the Transport of diluted species in porous media interface in the Chemical species transport module were used to build the model in COMSOL. The model was first calibrated using part of the experimental data for CO_2 permeability (6, 8 and 10 MPa injections under 11 and 17 MPa axial loads) and validated using the rest of the data. It was noted that the CO_2 permeability values of coal predicted by the model were consistent with the experimental results. Next, the model was extended to different injection pressures and axial loads to observe the behaviour of a thin coal seam during CO_2 sequestration. The following major conclusions were drawn from the model results. **9**CO_2 permeability through the coal mass is negatively affected by both CO_2 pressure and the depth of the coal seam, and this effect is decreased for greater depths and CO_2 pressures.

- CO_2 pressure distribution along the coal sample can be predicted reasonably well by the COMSOL model. Further, the flow parameters, such as CO_2 pressure and CO_2 concentration, reduce along the sample length with greater depths, and this is related to pore volume shrinkage caused by increased effective stress application.
- However, for a given axial load, CO_2 concentration increases with the increase in injection pressure, and this is due to the increase in net advective CO_2 flux with the increase in injection pressure.

Table 4: Error between the experimental and model-predicted total adsorbed CO_2 weight

Axial load (MPa)	CO_2 injection pressure (MPa)	Experimental value (kg)	Model predicted value (kg)	Error (%)
11	**6**	**0.75**	**0.71**	**5.33**
	8	**0.87**	**0.92**	**-5.82***
17	**6**	**0.64**	**0.60**	**6.25**
	8	**0.67**	**0.61**	**7.46**

***Negative sign means that the model-predicted value is higher than the experimental value**

.

- The CO_2 storage capacity in coal mass from the experiments and the model estimations followed a similar behaviour, showing an increase in cumulative adsorbed CO_2 weight with time. In addition, the experimentally-derived total CO_2 adsorption 10 days after approaching steady-state condition deviated by <8% from the model predictions.
- According to the model results for different CO_2 pressures and depths, greater amounts of CO_2 can be sequestrated into coal seams even at higher depths and higher CO_2 pressures despite the flow reduction observed if a sufficient time is allowed for CO_2 permeation.

ACKNOWLEDGEMENT

The authors wish to express their appreciation for the funding provided by the Australian Re-search Council (DE130100124).

REFERENCES

1. Anggara, F., Sasaki, K., Sugai, Y., 2013. Swelling Meas-urements of a Low Rank Coal in Supercritical CO2. International Journal of Geosciences 4, 863-870.
2. Day, S., Fry, R., Sakurovs, R., 2008. Swelling of Austral-ian coals in supercritical CO2. International Jour-nal of Coal Geology 74, 41-52.
3. De Silva, P.N.K., Ranjith, P.G., 2013. Advanced core flooding apparatus to estimate permeability and storage dynamics of CO2 in large coal specimens. Fuel 104, 417-425.
4. De Silva, P.N.K., Ranjith, P.G., 2014. Understanding the significance of in situ coal properties for CO2 se-questration: An experimental and numerical study. Int J Energ Res 38, 60-69.
5. Hol, S., Peach, C.J., Spiers, C.J., 2011. Applied stress re-duces the CO2 sorption capacity of coal. Interna-tional Journal of Coal Geology 85, 128-142.
6. Jasinge, D., 2010. An investigation of the effect of car-bon dioxide sequestration on the behaviour of brown coal (PhD thesis). Monash University, Mel-bourne, Australia.
7. Liu, G., Smirnov, A.V., 2009. Carbon sequestration in coal-beds with structural deformation effects. En-ergy Conversion and Management 50, 1586-1594.
8. McLinden, M., Klein, S., Lemmon, E., Peskin, A., 1998. REFPROP, Thermodynamic and transport proper-ties of refrigerants and refrigerant mixtures. NIST Standard Reference Database 23.
9. Nasvi, M.C.M., Ranjith, P.G., Sanjayan, J., 2014. A nu-merical study of CO2 flow through geopolymer under down-hole stress conditions: Application for CO2 sequestration wells. Journal of Unconven-tional Oil and Gas Resources 7, 62-70.
10. Perera, M.S.A., Ranjith, P.G., Choi, S.K., Bouazza, A., 2013. A parametric study of coal mass and cap rock behaviour and carbon dioxide flow during and after carbon dioxide injection. Fuel 106, 129-138.
11. Perera, M.S.A., Ranjith, P.G., Choi, S.K., Airey, D., 2011. The effects of sub-critical and super-critical car-bon dioxide adsorption-induced coal matrix swelling on the permeability of naturally frac-tured black coal. Energy 36, 6442-6450.
12. Perera, M.S.A., Ranjith, P.G., Choi, S.K., Airey, D., 2012. Investigation of temperature effect on permea-bility of naturally fractured black coal for car-bon dioxide movement: An experimental and numerical study. Fuel 94, 596-605.
13. Ranathunga, A., Perera, M., Ranjith, P., Ju, Y., Vishal, V., De Silva, P., 2015. A macro-scale experi-mental study of sub-and super-critical CO2 flow behaviour in Victorian brown coal. Fuel 158, 864-873.
14. Ranathunga, A.S., Perera, M.S.A., Ranjith, P.G., De Sil-va, G.P.D., 2016. A macro-scale view of the fluence of effective stress on carbon dioxide flow behaviour in coal: an experimental study. Geomechanics and Geophysics for Geo-Energy and Geo-Resources, 1-16.
15. Ranathunga, A. S., Perera, M. S. A., Ranjith, P. G., Zhang, X. G., & Wu, B. (2017). Super-critical carbon dioxide flow behaviour in low rank coal: A meso-scale experimental study. Journal of CO2 Utilization, 20, 1-13.
16. Ranjith, P.G., Perera, M.S.A., 2011. A new tri-axial ap-paratus to study the mechanical and fluid flow aspects of carbon dioxide sequestration in geo-logical formations. Fuel 90, 2751-2759.
17. Zhou, L., Feng, Q., Chen, Z., Liu, J., 2012. Modelling and upscaling of binary gas coal interactions in CO_2 enhanced coalbed methane recovery. Pro-cedia Environmental Sciences 12, 926-939.

Effect of salinity on the rate of consolidation of Sri Lankan soft peat

T. Jayasinghe[1], U.P. Nawagamuwa[2] and K.H.S.S. De Silva[3]

1 Department of Civil Engineering, University of Moratuwa, Sri Lanka
2 Department of Civil Engineering, University of Moratuwa, Sri Lanka
3 Central Engineering Consultancy Bureau, Sri Lanka

ABSTRACT: Peat is considered as a problematic geotechnical material with high organic content, moisture content, low shear strength, and high compressibility. There are around 1012 ha of marshy land underlain by peat in and around Colombo, Sri Lanka. Further, the peaty soils found in Sri Lanka are generally of the amorphous type due to their low organic content. Intrusion of salinity into the low-lying marshy lands has become a serious threat and this study presents the impact of variation in salinity of water on the rate of consolidation of soft peat found in Kaduwela, Sri Lanka. The salinity level in the selected peat specimen was altered with addition of salt grains, to observe the variation of rate of consolidation with salinity. Test specimens were prepared by air drying the mechanically mixed peat samples after removing decayed particles. These pre-prepared disturbed samples were tested with different salt amounts (0, 5, 10, 15 and 20%). Kaolin clay was used as the controlled specimen and it was observed that the salinity variation had no considerable effect on kaolin as it is considered a neutral clay. All samples were tested in the odometer with different loading and it was observed that the rate of consolidation of peat can be increased with the addition of salt grains, however, the optimum amount of salt addition is within 10-15% by weight of the initial peat sample for an increased rate of consolidation. Chemical properties (Sulphate and Chloride content), organic content and pH value of test samples were also observed with the addition of salt, whereas only chloride content showed a considerable change which is anticipatory with the addition of salt grains.

Key Words: *Consolidation, Peat, Sol unity*

LIST OF NOTATIONS

c_α	coefficient of secondary compression
c_c	compression index
c_v	coefficient of consolidation
m_v	coefficient of volume compressibility
K	kaolinite sample/s
OC	organic content
P	peat sample/s

1. INTRODUCTION

Consolidation settlement in general is related to soft soil types such as clay, peat or organic soils. With the drastic increase in population and land consumption, availability of good lands with good soil conditions for construction is less. Therefore, civil engineering structures and other infrastructure facilities are to be constructed on unfavourable sub soils such as soft clays, soft organic clays and peat. 1012 ha of marshy land underlain by peat can be found in and around Colombo, Sri Lanka. Prior to construction often these sites are improved using various ground improvement methods and use of earth fills is the most common approach. With the weight of the fill and the proposed structure, soft soil underneath will experience large consolidation settlements. This makes a serious issue in geotechnical engineering and there are several methods prevailing to over-come this problem. Limitations in these methods are mainly consumption of time and consumption of large amounts of money. This raises the need of development of new methods of ground improvement. Previous studies have been addressing this issue with addition of salt grains to improve the rate of consolidation and has found that there is a considerable increase in rate of consolidation with the increase of salinity level in peat. Therefore, the main objective of this study is to develop a quantitative analysis of the effect of salinity of water on the rate of consolidation of Sri Lankan soft peat and application of the results on practical situations. As a secondary objective, influence of salinity on parameters of consolidation will be studied, along with the variation of selected chemical and physical properties of the soil. As salt is a natural resource which is available in Sri Lanka, addition of salt to improve amorphous peaty soil found in Sri Lanka is an economic ground improvement method along with the current practices like preloading.

1.1 Peat

According to Karunawardena (2007), peat generally refers to natural material which is composed primarily of plant material in various stages of decomposition and characterized by high compressibility and low shear strength. Further, peat is normally considered as a problematic geotechnical material due to its low shear strength, high compressibility and high water content. Kazemian (2011) stated that the 75% of its contents are organic. Peat consists of fragmented organic materials formed in wet-lands under suitable climatic and topographic conditions and is formed from vegetation that has been chemically changed and fossilized (Dhowian and

Edil, 1980). Further, peat is formed in low-lying, waterlogged areas or in lakes or ponds with extremely poor drainage when organic (usually plant) matter accumulates more quickly than it humidifies (Karunawardena, 2007). Peat does not contain any form of strength favourable in constructions (Munro, 2005). Dominant factors controlling the compressibility of peat are fibre content, water con-tent, void ratio, permeability, arrangement of soil particles and inter particle chemical bond in some soils (Mesri and Ajlouni, 2007). The organic content of peat is also an important geotechnical parameter, since it influences most of the peat's physical and mechanical properties (Karunawardena, 2007). Compression pattern of peat differs from the compression patterns of other soil types mainly in two ways. The com-pression of peat is much larger than that of oth-er soils and a significant amount of total settle-ment of peat consists of the creep settlement than of other soil types (Kazemian, 2011). According to Karunawardena (2007), the secondary compression is more significant in peaty soils than in inorganic clays and the reason for the above characteristic of peat is the relatively short duration of primary consolidation due to the high initial permeability.

1.2 Properties of Sri Lankan peat

In Sri Lanka, the fluctuation of the water table, due to excessive rainfall, provides suitable conditions for the accumulation of peat deposits in the areas near Colombo which consist of poorly drained grounds. This process has been occurring for a long time and, as a result, there are now around 1012 ha (2500 acres) of marshy land underlain with peat in and around Colombo (Karunawardena, 2007). Also, ac-cording to him, the peaty soils found in Sri Lanka are generally of the amorphous type due to their low organic content

Table 1: Basic properties of Sri Lankan peat (Karunawardena, 2007)

Peat type	Amorphous peat
Water content	200%-800%
Initial void ratio	2.0-8.0
Organic content	20%-50%
Specific gravity	1.5-2.2
pH value	Less than 3.0
Liquid limit	Often less than the natural water content (%)

According to the same research stated above, it has been found that the compressibility and creep characteristics of the peat found in Sri Lanka is directly proportional to the organic matter content. Figure 1 and 2 displays the vari-ation of c_c and c_α with the organic content of Sri Lankan peat.

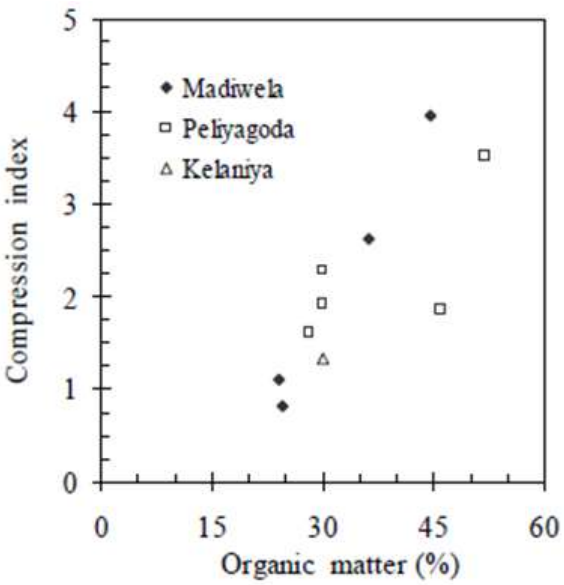

Figure 1: Cc vs. OC (%) relationship for Sri Lankan peats (Karunawardena, 2007)

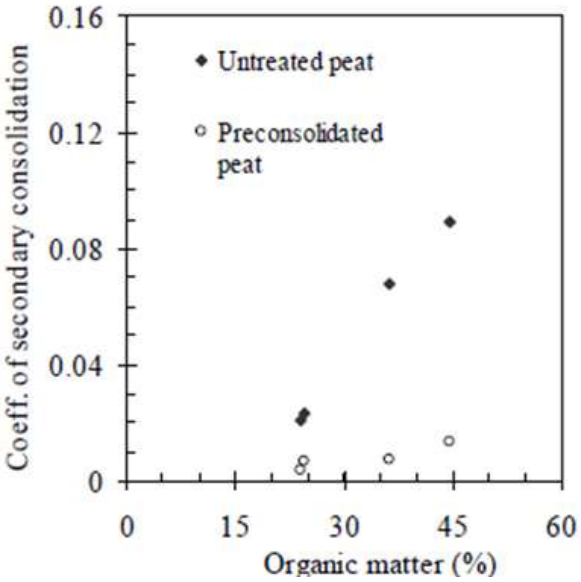

Figure 2: Cα vs. OC (%) relationship for Sri Lankan peats (Karunawardena, 2007)

1.3 Factors affecting consolidation of peat

The compression or consolidation settlement of a soft soil depends on factors such as struc-ture and fabric, stress path, temperature and loading rate (Leroueli, 1996). Though the ap-propriate relations and the corresponding mate-rial parameters can be identified with laboratory tests, sample disturbances caused due to stress release, temperature variations and variations in moisture content can have a significant effect on compressibility of a soft soil (Crawford, 1965). Kuhn and Mitchell (1993) states chemi-cal characteristics of soils such as the amount and type of anaions and the existing cations have a substantial impact on the physical and mechanical behavior including

consolidation. Under similar test conditions of one dimension-al loading, fibrous peat can be improved with intrusion of little amount of salt grain (Zhang and O'Kelly, 2015). They have assessed the macropore structure of peat once salt grains are added. When salt grains are added to the fi-brous peat specimen, Sodium and chloride ions are released around the surface of the salt grains by the ionisation process as illustrated in Figure 3.

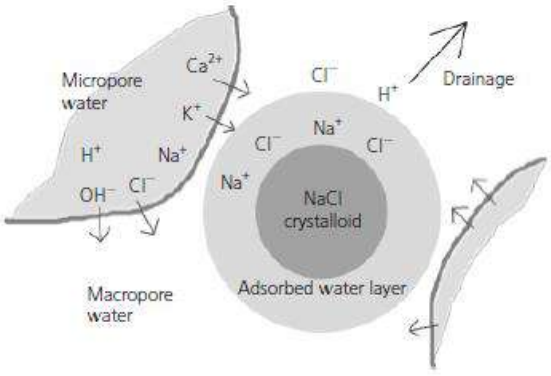

Figure 3: Sodium chloride grain dissolving in peat macropores (Zhang and O'Kelly, 2015)

When salt grains are added micro-pore water can transfer to macro-pores quicker and that makes pore water ready to drain due to loading gathers around the salt grains during ionization. With this the consolidation process of the peat is accelerated by quickening drainage during the ionization process. Presence of sodium ions in the peat specimen assists in the release of more free water molecules from the peat structure. Further Zhang and O'Kelly (2015), states that Sodium chloride salt was selected for the study as it has a neutral pH. According to Pichan and O'Kelly (2012), increases in pH value of the pore water in peat can cause an increase in the rate of decomposition of constituent organic matter, which can affect the composition of the fibrous peat.

When the addition of salt grains is studied, Zhang and O'Kelly (2015) have concluded the effect of salt grain size for an acceleration of the consolidation rate for fibrous peat. Accord-ing to their study, the period over which the salt grains remain undissolved in water is the period of the salt treatment. Therefore, once the salt is fully dissolved in pore water of peat, the effect on consolidation is marginal, leading to the con-clusion that fine salt will have shorter active pe-riods compared to coarse grained salt. This indi-cates the necessity of appropriate grading of salt gains for an acceleration of consolidation of fi-brous peat.

Zhang and O'Kelly (2015), have observed that the rate and the magnitude of primary con-solidation settlement of the soil specimen and the coefficient of permeability increases with the addition of salt grains. Further, the creep set-tlement is also reduced, as greater settlements are taking place during the pre-primary consoli-dation stage. De Silva and Nawagamuwa (2016) have stated that under similar test conditions of one dimensional loading amorphos peat shows an increase in consolidation with increased salinity levels. Fahy (2014) has identified that the time for the end of primary consolidation rate was inversely proportional to the salinity in pore fluid of high plasticity soils.

2. METHODOLOGY

2.1 Sample collection and test materials

The experimental procedures were conduct-ed on a peat sample extracted from Kaduwela, Sri Lanka. Kaolin clay was used as the control specimen, which is identified as a soil type without any noteworthy influence with salt grain addition as kaolin has the properties of natural pozzolan (Wong et al, 2012).

2. 2 Sample preparations for oedometer test

The collected soil mass was mixed mechani-cally to make the sample even, after manual removal of hard particles such as stones, plant matter and decayed particles which were pre-sent in the soil. Then the mixed sample was air dried for 24 hours (Figure 4).

Figure 4: Mechanically mixed peat sample

The air-dried sample was then divided in to 5 approximately equal masses of around 450g. Salt grains (passing no 40 seive) were then added in to each of the soil masses in the selected salinity levels, 0, 5, 10, 15, and 25% by initial weight of the air-dried sample and was allowed for setting. Having added salt, the sample was mixed properly using manual techniques until it gets settled and then mechanical mixing was conducted for about 4 minutes using an electric beater until the soil is mixed evenly. Distilled water was added while mixing in small portions until the mixture gets a proper workable texture. Once the mixture is ready, sample was prepared in a separate plastic bowl carefully, while max-imum attention was being paid to minimize any air void formation (Figure 5).

Figure 5: Careful preparation of the sample in separate bowls

Then the prepared sample was covered by a wet filter paper and placed in an air tied polythene bag for 24 hours to avoid any moisture loss. Then the sample was carefully extracted in to the odometer ring for the testing. Odometer samples were submerged in distilled water to avoid any changes in saline concentration from the other sources. The moisture content of the prepared peat samples (P) were within 140%-185% which was obtained using oven drying the samples at 65^0 C.

Kaolin samples (K) were also prepared in the same manner for oedometer test keeping the moisture content of the samples within 60%-70% which was the optimum moisture content of kaolin.

2.3 Tests performed

As preliminary tests, sieve analysis (ASTM D 6913) and hydrometer analysis according to ASTM D422-63(2007) were used to identify the particle size distribution of unsalted peat ample (P_0). Organic content test according to ASTM D2974–14, specific gravity test according to ASTM D792 and chloride and sulphate tests ac-cording to BS 1377: Part3:1990 were also con-ducted on P_0.

After the preliminary testing, the samples (P and K) were kept for two days to settle in the new environment in the oedometer ring and a series of one-dimensional consolidation tests (oedometer tests) was conducted according to ASTM D4546. Oedometer tests were carried out for both peat and kaolin clay samples which were prepared in the above mentioned procedure. Five number of disturbed soil samples from each soil type (P and K) were tested with different salinity levels.

In test stage 1, testing was done with loading stages of 5, 10, 20 and 40 kNm-2 incremental loading after 24 hour time interval. Unloading was done in one stage only. In test stage 2, oe-dometer tests were carried out only for 2 select-ed peat samples, i.e.; 0 and 15%. 15% of salt addition was selected since, there was no change to cv values from 24hr oedometer tests after 15% of salt addition. 0% was selected as a control sample to compare the results. In stage 2, loading and unloading was done in the same stages as in test stage 1, but load incrementing and decrementing was done in 7 day interval to observe the impact of salinity on secondary consolidation. The readings of the tests were recorded as per the standards (BS 1377:5) of odometer test.

Chloride, Sulphate and pH tests were per-formed for all the peat samples with varied salinity levels which were tested in odometer and on the initial peat samples. Tests were conducted according to BS 1377: Part 3 (1990).

3. TEST RESULTS AND ANALYSIS

Figure 6 illustrates the particle size distribution of peat (P_0) sample. Test results of preliminary tests performed on the same P_0 sample is presented in Table 2.

Table 2: Test results of preliminary tests performed on the P_0 sample

P_0	
Sulphate content	5%
Chloride content	0.02%
Water content	175%
Organic content	41%
Specific gravity	2.2

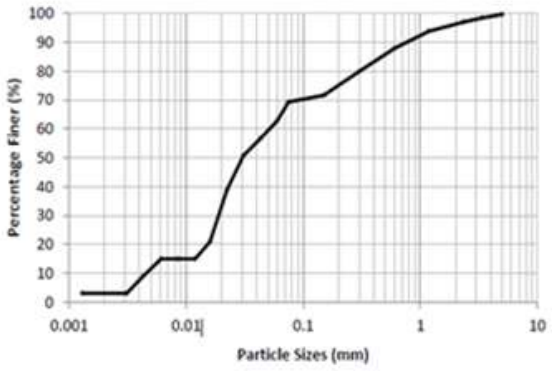

Figure 6: Particle size distribution of P_0 sample

Kaolin and peat samples are hereafter referred to as their salt content added by weight. I.e. 0, 5, 10, 15 and 25%. Figures 7 and 8 illustrate the settlement against square root time for P and K samples.

According to one dimensional consolidation theory developed by Terzaghi (1925) to interpret soil consolidation, coefficient of consolidation (c_v), coefficient of volume compressibility (mv), compression index (c_c) and secondary compression index (c_α) of the above samples were determined for each stage of loading (Budhu, 2008). c_v was determined using square root time method (Taylor, 1942) due to the difficulties found in determining the c_v value from log time and hyperbolic

methods, which are the alternative methods of finding c_v value for each loading step.

3.1 Effects of salt addition on primary consolidation properties

Figure 7 and 8 represent the settlements corresponding to all the loading stages for P and K samples respectively. Figures 9, 10, 11, 12 illustrate coefficient of consolidation (c_v) from square root time method (for K and P samples), coefficient of volume compressibility (m_v) (for P and K samples) respectively.

Figures 9 and 10 show the impact of the addition of salt in both kaolinite and peat on coefficient of consolidation. According to K sample results, it can be concluded that the addition of salt grains has not considerably influenced the results in K sample set. However, in Figure 10, it is clearly visible that the addition of salt grains has altered the coefficient of consolidation of peat samples. When considering the variation of c_v with the loading stage, it shows a reduction of c_v and then an increase. There is a change in the trend around 10-20 kNm^{-2} loading stage. When the variation of c_v with the salt addition by weight is considered, c_v has different variations for different loading stages. However, after 15% of salt addition onwards, c_v becomes constant.

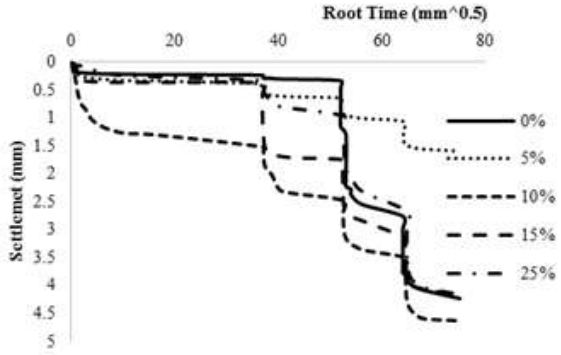

Figure 7: Oedometer test results of P

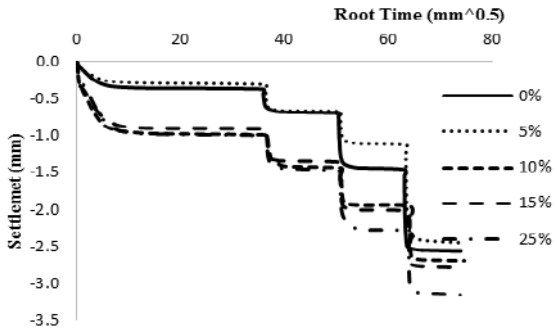

Figure 8: Oedometer test results of K

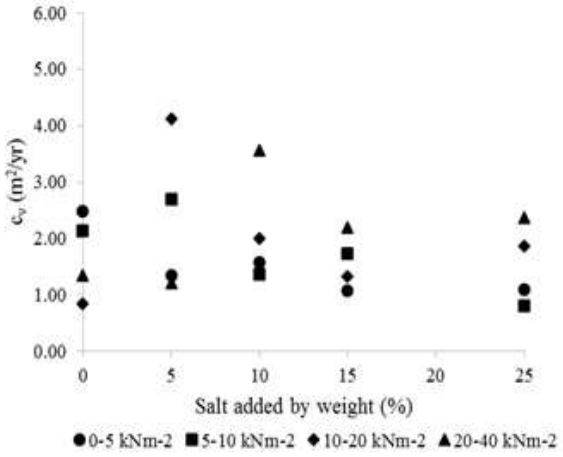

Figure 9: Variation of c_v of K sample with salt added by weight

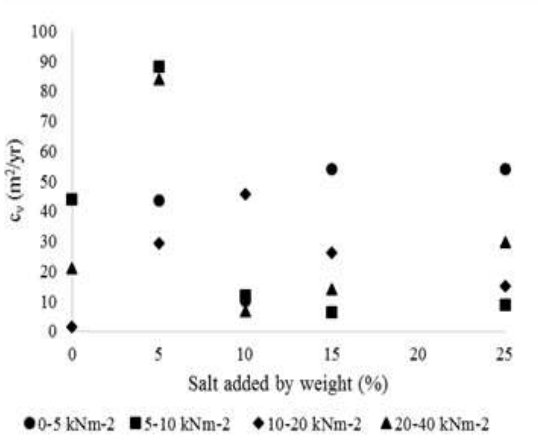

Figure 10: Variation of c_v of P sample with salt added by weight

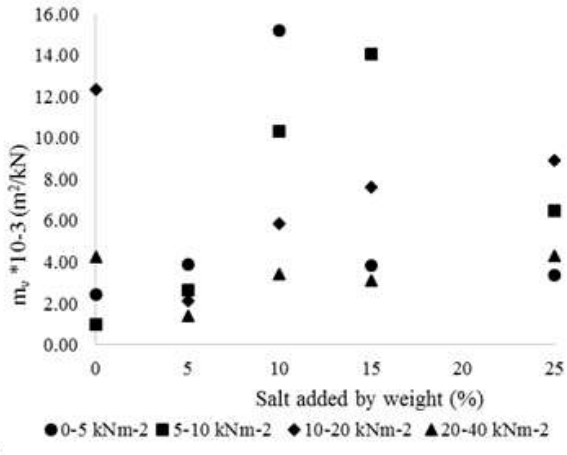

Figure 11: Variation of m_v of P sample with salt added by weight

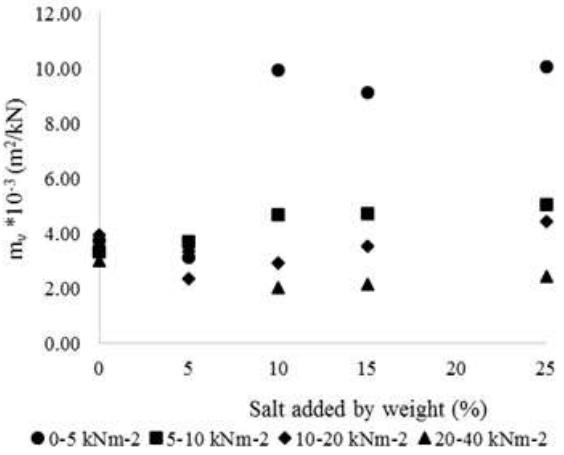

Figure 12: Variation of m_v of K sample with salt added by weight

Figure 11 represents the effect of salt grain addition on the volume compressibility of P. It shows that m_v of peat is increasing till 10 -15% of salt addition by initial weight and then de-creasing to initial m_v (m_v at 0% salt) in each loading stage. According to K result set as in Figure 12, the m_v of K sample does not show a meaningful change with the addition of salt when compared with the peat sample.

Table 3. Compression index (c_c) of P and K samples

Salt added by weight %	c_c	
	P	K
0	1.26	0.49
5	0.41	0.55
10	0.80	0.29
15	0.74	0.28
25	0.94	-

According to Table 3, compression Index (c_c) of peat sample set has been decreased and then increased with the amount of salt added by weight. The turning point is around 5% of salt added by weight. c_c values presented by Karunawardena, (2007) for an organic content of 40-46% have much higher values than that of the original peat sample of this study with 0% salt by weight. But this can be due to the test procedures and sample preparation techniques where the sample disturbance affects the rate of consolidation. However, K samples do not show a significant variation of c_c with salt addition. But the compression index values in peat sample set are higher than that of K samples. Therefore, these comparisons confirm that the effect of salinity on consolidation is considerably higher in peaty soil types while it has a low impact on non-organic neutral clays like kaolin.

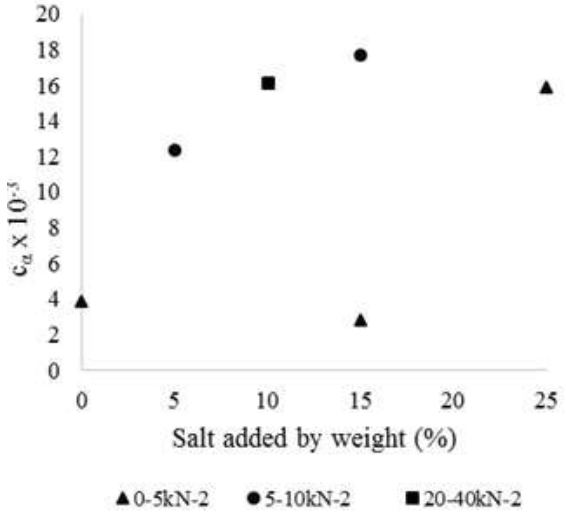

Figure 13: Secondary compression index (c_α) of P sample

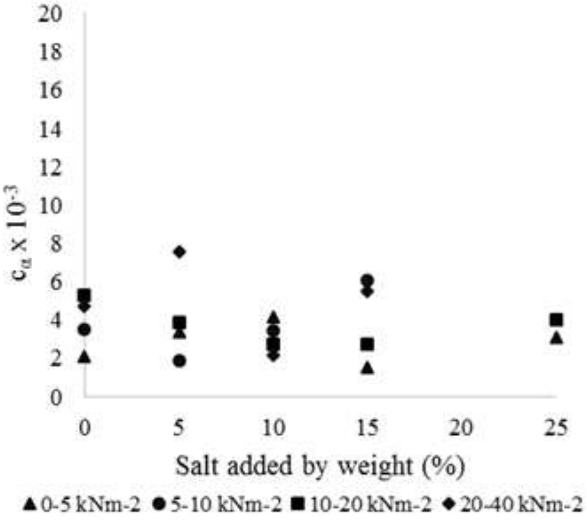

Figure 14: Secondary compression index (c_α) of K sample

3.2 Effects of salt addition on secondary consolidation properties

Results of secondary compression index (c_α) of peat samples shown in Figure 13 are not ad-equate to conclude any behaviour pattern of c_α with addition of salt. When the existing results are compared with the results of Karunawardena, (2007), it can be recognized that the c_α of all the peat samples falls into the trend of untreated peat rather than pre-consolidated. However, according to Figure 14, it can be concluded that the secondary compression index, c_α of kaolin clay does not vary significantly with the addition of salt.

Further, Figure 7 clearly shows that the rate of secondary consolidation (creep) also has in-creased with the addition

of salt grains. K sample does not show any such significant creep settlement as shown in Figure 8.

Table 4: Results of Chloride, Sulphate, organic content and pH tests

Salt added by weight %	Sulphate content (%)	Chloride content (%)	Organic content (%)	pH value
0	0.63	0.02	42	3.11
5	0.66	0.62	41.83	3.23
10	0.65	1.1	43.42	3.31
15	0.58	1.65	44.1	3.5
25	0.55	1.92	46	3.72

According to Table 4, sulphate content in the P samples are in a close range while the chloride content is increasing with the addition of salt, which is well anticipated. Organic content of the samples is similar and confirms that the samples are almost identical.

4. CONCLUSIONS

This study concludes that the effect of salinity on the rate of consolidation of peat is considerable compared to kaolin clay which is inorganic. Under similar conditions of one dimensional loading, the primary consolidation settlement of peat has become greater and faster in magnitude with the addition of salt grains. The effect is increased with the amount of salt addition to a certain extent and the effect seems to become decreasing with further addition of salt. Therefore, for an increased rate of consolidation of peat, the salinity level must be within 10 -15% of salt by weight of the initial sample ac-cording to the observations of this research. Further, cv has increased and has become constant after saline level of 15% (by weight), mv appears to become constant after 15% of salt addition by initial weight while cc of peat de-creases and increases with the amount of salt added by weight. However, this data is not adequate to predict the latter effect accurately. Furthermore, the results end up with insufficient information to predict the effect of salt addition on the secondary consolidation of peat since the c_α values for all the loading stages couldn't be determined due to the complex secondary consolidation process of peaty soils.

However, salt intrusion into natural peat de-posits can be a threat to the existing environ-mental conditions and bio-diversity of such peat swamps. Further, methods and limitations of salt mixing with natural peat has to be studied thoroughly in order to implement this type of ground improvement in practice which is be-yond the scope of the current study.

ACKNOWLEDGEMENTS

Staff members of soil mechanics and environmental engineering laboratories in the Department of Civil Engineering, University of Moratuwa are gratefully acknowledged.

REFERENCES

1. ASTM D2974 -87 – Standard Test Methods for Moisture, Ash, and Organic Matter of Peat and Organic Soils
2. ASTM D422-63 Standard Test Method for Particle-Size Anal-ysis of Soils (2007)
3. ASTM D4546-96 Standard Test Methods for One-Dimensional Swell or Settlement Potential of Cohesive Soils
4. ASTM D6913-04 Standard Test Methods for Particle-Size Dis-tribution (Gradation) of Soils Using Sieve Analysis.
5. ASTM D792-08 Standard Test Methods for Density and Spe-cific Gravity (Relative Density) of Plastics by Displace-ment.
6. Budhu, M., 2008. Soil mechanics and foundations. 2nd Edition ed. s.l.:Wiley India Pvt. Ltd.
7. BS 1377-3: 1990 Methods of test for soils for civil engineering purposes. Chemical and electro-chemical tests.
8. BS 1377-5: 1990 Methods of test for soils for civil engineering purposes. Compressibility, permeability and durability tests.
9. Crawford, C.B., 1965. The Resistance of Soil Structure to Con-solidation. Canadian Geotechnical Journal, 2(2), pp.90–97.
10. De Silva K.H.S.S., and Nawagamuwa, U.P. 2016. Effect of sa-linity on consolidation of peat, Civil Engineering Research Symposium Moratuwa (CERS2016), December 2016.
11. Dhowian, A. & Edil, T., 1980. Consolidation Behavior of Peats. Geotechnical Testing Journal, 3(3), p.105.
12. Fahy, B.P., 2014. The influence of salinity on the mechanical behavior of high plasticity soils. Thesis.Karunawadena, A., 2007. Consolidation Analysis of Sri Lankan peaty clay using elasto - viscoplastic theory.
13. Kazemian S., Bujang B.K. H., Prasad A., Barghchi M., 2011. A state of art review of peat: Geotechnical engineering perspective. International Journal of the Physical Sciences, Volume Vol. 6(8), pp. 1974-1981.
14. Kuhn, M.R. & Mitchell, J.K., 1993. New Perspectives on Soil Creep. Journal of Geotechnical Engineering, 119(3), pp.507–524.
15. Leroueil, S., 1996. Compressibility of Clays: Fundamental and Practical Aspects. Journal of Geotechnical Engineering, 122(7), pp.534–543.
16. Mesri, G. & Ajlouni, M., 2007. Engineering Properties of Fi-brous Peats. Journal of Geotechnical and Geoenvironmen-tal Engineering, 133(7), pp.850–866.

17. Munro, N., 2005. Dealing With Bearing Capacity Problems on Low volume roads constructed on peat. ROADEX II Northern Periphery.
18. Pichan, S., & Okelly, B. 2012. Effect of Decomposition on the Compressibility of Fibrous Peat. GeoCongress 2012. doi:10.1061/9780784412121.445.
19. Taylor, D. W., 1942. Research on consolidation of clays. Serial No. 82, Massachusetts Institute of technology, Cambridge.
20. Terzaghi, K., 1925. Erdbumechanik. Franz Deuticke, Vienna.
21. Wong L.S, Hashim R. & Ali F., 2012. Improved strength and reduced permeability of stabilized peat: Focus on applica-tion of kaolin as a pozzolanic additive. Construction and building materials, 40(2013), pp. 783-792.
22. Zhang, L. and O'kelly, B.C., 2015. Effect of salt grain additions on fibrous peat consolidation. Proceedings of the Institu-tion of Civil Engineers - Ground Improvement, 168(1), pp.14–21.

Study of pullout resistance of soil nails in tropical residual soils

W.E.P. Ranjan Kumara[1] and S.A.S. Kulathilaka[2]

1 *Central Engineering Consultancy Bureau, No. 415, Bauddaloka Mawatha,Colombo-07,Sri Lanka*
2 *Department of Civil Engineering, University of Moratuwa, Sri Lanka*

ABSTRACT: The pullout resistances in soil nailing designs are estimated using available empirical formulae or theoretical formulations. Occasionally these are revised through pullout tests done at early stages of the design. In Sri Lanka pullout tests are mostly done as proof tests after completion of a project. When a pullout test is done on a working nail, the resistance developing over the full length of the nail exceeds the tensile strength and it could never be subjected to loads close to their pullout capacity. In a project eight nails were installed with short grouted lengths and all the nails were completely pulled out after being subjected to three loading/unloading/reloading cycles. The shear strength parameters of the soil forming the slope were obtained by testing undisturbed samples under both natural and saturated conditions. These parameters were used in currently available design formulae to estimate a pullout resistance which was then compared with the experimentally determine values. The experimental values were found to be generally greater than the calculated value. The diameter of the pulled out grouted body was found to 20% more than the nominal diameter. When the effects of; matric suction (estimated), possible dilation effects and increase in diameter were accounted for the two values became much closer.

Key Words: *Pullout resistance, Residual soil, Soil nails*

1. INTRODUCTION

Soil nailing is a widely used slope stabilization technique utilizing reinforcement bars encased in a grouted bore hole oriented in a slightly downward direction from horizontal. When the soil mass attempts to move down tensile forces mobilized in the intercepted nails will enhance the shear resistance by increasing the normal stress along the potential failure surface. The shear stresses to be mobilized by the soil are also reduced. The tensile force that can be provided by the nail depends on the tensile capacity of the reinforcement bar and the pullout resistance at the interface of the grouted body and the natural soil. The ultimate pull-out capacity of soil nails depends primarily on; strength characteristics of the soil, installation technique, geometry of drilled hole and the grouting method. The soil nailing technique has been found to be suitable for supporting excavations, tunnel portals, slope stabilization, bridge abutments and several other civil engineering applications. The technique has been utilized increasingly in recent years due to its technical and economic advantages. The equipment used for soil nailing are quite light facilitates quick and easy construction and contribute to significant savings (Powell and Watkins, 1990).

The shear strength at the nail-soil interface and hence the pull-out resistance is affected by several critical factors such as; soil type, drilling method, characteristics of grout, overburden pressure, soil density, soil dilatancy,

and degree of saturation (Burland, 2002). Several research studies have been conducted to investigate the behavior of the soil-nail interface during pull-out (Chai et al., 2004; Junaideen et al., 2004; Chu and Yin, 2005; Yin et al., 2006; Pradhan et al., 2006; Sivakumar and Singh, 2010). It was reported by Zhang et al. (2009) that matric suction is a key factor that contributes to the uncertainties in the estimation of the pull-out capacity of soil nails. Gurpersaud (2010) studied the influence of the matric suction on pullout capacity of soil nailing with laboratory model studies on a compacted sandy soil.

In this study test nails were installed in a slope in an unsaturated condition. Nails were made short to ensure that they will be pulled out without causing tensile failure. The actual pullout resistance and grouted perimeters of the nails pulled out were measured. Undisturbed soil samples were taken from the corresponding locations of the test nails to establish shear strength characteristics.

The key objective of this study is to compare the observed pullout resistances with the formulae currently being used in the design practice and find ways to improve the design estimates.

2. ESTIMATION OF PULLOUT RESISTANCE

Numerous field and laboratory tests have been performed to investigate the pull-out behaviour of soil nails by several investigators. Design charts were proposed to estimate the pull-out capacity of grouted and driven nails in various types of soils based on a number of field pull-out test results performed during the French National Research Project - "Clouterre" (FHWA, 1993). Several researchers also conducted studies to evaluate soil-nail interaction by using a large direct shear box (Chu and Yin, 2005; Sivakumar and Singh, 2010). Milligan and Tei, (1997) attempted to study the effects of initial stress in the soil, grouting pressure and stress changes during the pull-out test. Several formulae developed through these researches will be compared with the experimental results of this research.

2.1 Factors affecting pullout resistance

2.1.1 Effect of dilatancy

Dilation occuring in dense sand during shearing can result in an increase in normal stress acting on soil nails during pull-out. If dilation is partly restrained by surrounding soils (restrained dilatancy), it will results in normal stress increase up to four times the initial stress (Schlosser 1983). Pradhan (2003) showed that the soil particles around the nail will dilate when the shear stress is applied on the soil nail interface during pull-out. Numerical simulation of the effects of dilatancy on soil nail pull-out resistance was performed by Su et al. (2008). The results suggest that soil dilatancy has a significant influence on the soil nail pull-out resistance. The dilation angle was added to the interface friction angle of the soil according to Coulomb's Model. Figure 1 shows the relationship of the average pull-out stress with (a) pull-out displacement and (b) dilation angle(ψ).

These results clearly show that the pull-out resistance initially increases quickly with the dilation angle. For dilation angles(ψ) greater than 10°, the pull-out resistance increases and then remains constant.

2.1.2 Effects of method of installation

The profile of the drilled hole for grouted nails will also influence the normal stress acting on the nail. A smooth cylindrical borehole will have normal stress equal to the stress prevailing during drilling (almost zero) and the resulting pull-out capacity will be low. An irregular drilled hole will develop a rib effect during grouting and mobilize restrained dilatancy effect, causing an increase in normal stress (Plumelle et al., 1990).

2.1.3 Effect of angle of internal friction of soil

Soil-nail interface coefficient depends on the properties of soil and nail surface characteristics. Franzen (1998) stated that an increase in the angle of internal friction, ϕ^1 /of the soil will result in greater mobilized friction between the nail-soil interface and hence results in an increase of the normal stress during pull-out. An increase in the coefficient of uniformity of the soil will generally result in an increase in the angle of internal friction $\phi^{/}$. The relative density is another factor affecting the angle of internal friction ϕ^1 /. Soils with a higher value of relative density have a greater tendency to dilate and contribute to an increase in the angle of internal friction (Franzen, 1998).

2.1.4 Effect of matric suction

Soils comprising cohesion and friction components were highly influenced by the variation in degree of saturation (i.e. variation in matric suction values). Schlosser(1983) reported that pull out resistance in clayey gravel reduced by 50% when the water content was increased from optimum water content to full saturation. This greater pull-out capacity at the optimum water content can be attributed to the contribution of matric suction.

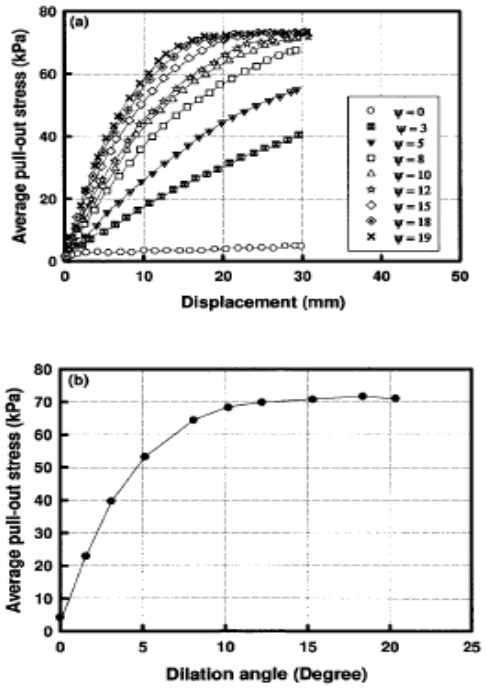

Figure. 1: Relationship of the average pull-out stress with pull-out displacement and dilation angle (Su et al 2008)

A series of laboratory pull-out tests were performed by Su et al., 2008 in completely decomposed granite (CDG) at different degrees of saturation. The test results showed that the peak pull-out strength of the soil nails was strongly influenced by the degree of saturation of the soil. Peak pull-out shear strength values were obtained between degrees of saturation of 50% and 75%. The pull-out capacity was found to decrease with increase in the degree of saturation.

Studies performed by Su et al., (2008) indicated that the effect of the degree of saturation on soil nail pull-out capacity is significant and should be carefully addressed in design of soil nailing system.

Gurpersaud (2010) conducted a comprehensive experimental program to understand the influence of matric suction on the pull-out capacity of compacted sand under both unsaturated and saturated conditions. A strong relationship was obtained between the Soil Water Characteristic Curve(SWCC) and pull-out resistance. As shown on Figure 2, this relationship demonstrates that there is a linear increase in the pull-out capacity up to the air-entry value, followed by a non-linear increase. The behavior of the pullout capacity matched the different phases of SWCC.

The texture of the soil nail surface will also influence the interface friction angle, $\phi^{/}$ An extremely rough surface will fail by pull-out within the soil outside the nail and the angle of the internal friction $\phi^{/}$ for the soil, will be the

governing parameter. A completely smooth nail will fail at the soil-nail interface and the angle of internal friction, ϕ' for the soil is governed by soil-nail interface friction, δ (Schlosser and Guilloux 1981).

Pull-out failure for most soil nails can be expected to occur partly as soil/soil and partly as soil/nail interface and the actual interface friction angle varies between and tan δ and tan ϕ'.

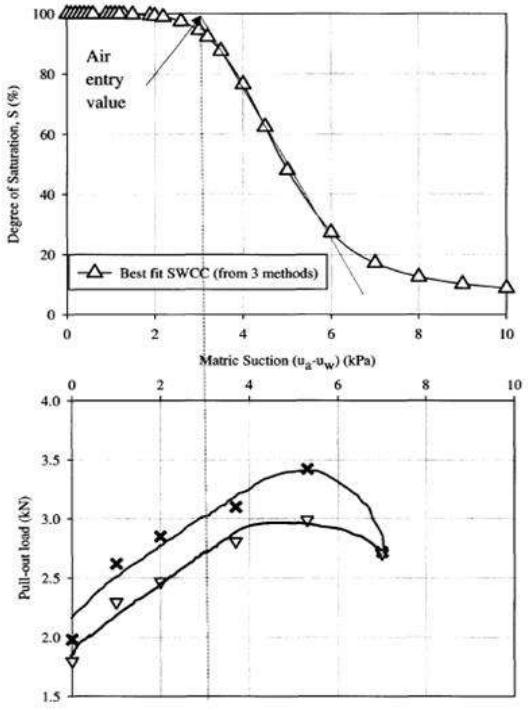

Figure 2: Pullout capacity Vs Matric suction (Gurpersaud 2010)

2.1.5 Influence of overburden pressure on Pull out resistance

Extensive research studies by Cartier and Gigan 1983; Heymann et al. 1992; Byrne et al. 1998; Franzen 1998; Franzen and Jendeby 2001 showed that the pullout resistance was independent of the embedded depth of soil nails. Li and Lo (2007), showed that after a drill hole is formed, the radial stress in the vicinity of the soil face of the nail hole is close to zero. After installation of steel bar and grouting, a small effective radial stress is introduced. In a pullout test, the resistance is developed mostly because of; dilation of soil during shearing, interface dilation from rough drill hole face and physical bonding at the soil-grout interface. Yeo et al. 2007 investigated the local stresses near the soil-nail interface by a numerical study. In the study, the construction procedures including drilling of the nail hole, insertion of the nail, grouting, and pullout of the nail were simulated. The numerical results showed that the radial stress along the nail-soil interface is initially very small due to the nail installation procedure and increases with pullout displacement. The radial stress generated by the pullout displacement is found to be strongly dependent on the dilation angle of the soil.

2.1.6 Effect of grouting pressure

In general grouting of soil nailing is done under low grouting pressures (gravitational grouting). However in some recent projects pressurized grouting has been used. Seo et al (2012) studied the effect of grouting pressure on pullout resistance. When the grout is injected to the cavity formed by drilling, the pressure exerted around the cavity perimeter was found to increase with time up to a peak value and reduce gradually to a residual value. The pressure reduction was attributed to the seepage of water originally retained in the grout into the adjacent soil formation. Seo et al (2012) found that with the application of pressurized grouting insitu stresses can be increased by approximately 20% of the injecting pressure. To develop a desirable residual stress in a soil nailing system, the grouting pressure should be maintained for a minimum injection time. The required time increases with the fines content and the pressure itself. It was established through field testing that pullout resistance was increased by 36% due to pressurized grouting. This increase was attributed to; enlarged diameter, higher roughness, compaction of soil near the grouted hole and increased dilatancy effects.

2.1.7 Comparison of Direct shear tests with pull-out test

The shear strength failure envelopes for pull-out tests and interface shear tests show trends similar to soil-soil direct shear test. The peak interface friction angle, $\boldsymbol{\delta}$ from the soil-grout interface shear tests is generally close to that of the soil nail pull-out tests. Based on results obtained by Chu and Yin (2005), the interface friction angle $\boldsymbol{\delta}$, of grouted nails can be estimated by using soil-grout interface shear tests. Pradhan et al., 2005 observed that the mobilization of shear stress in the direct shear test is similar to that of the laboratory pull-out test until the first slip occurs for CDG. Figure 3, shows a comparison of results obtained from pull-out tests and direct shear test for CDG.

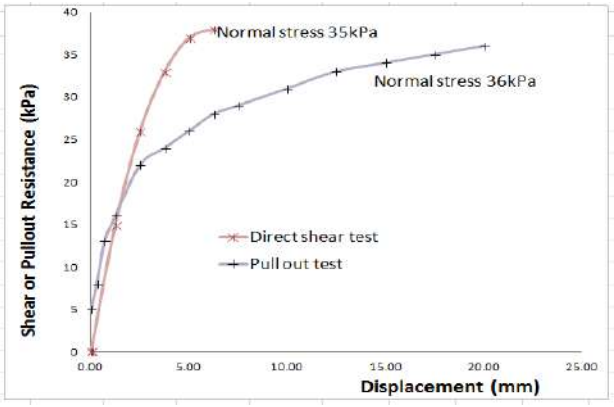

Figure 3: Pull out test Vs Direct Shear test results

3. EXPERIMENTAL EVALUATION OF PULLOUT RESISTANCE

In order to obtain a realistic comparison between the theoretical and actual results for the pullout resistance, it was decided to install several soil nails in actual site conditions.

A slope in the premises of the Kegalle hospital was to be stabilized by the installation of soil nailing. Along with the project, it was decided to have eight test nails for the determination of the pullout resistance. The test nails were not a part of the original design required for stabilization. Thus, it was possible to load the nails up to the point of failure.

The slope under consideration was a cut slope with an inclination of 75^0 to the horizontal axis, and of width of approximately 24m and height 10.5 m with certain indications of instability. The natural terrain above the slope was with a 30^0 `slope to the horizontal, and was in a stable state. A soil nailing design was done to enhance the stability of the slope. The design required 84 nails to be installed into the surface. The inclinations of the nails were 15^0 to the horizontal. The nails were 25mm diameter tor steel reinforcement bars of lengths varying between 7-9m. The nominal diameter of the drill hole was 116 mm. The nail locations and the arrangement is presented Figure 4.

Figure 4: Proposed nailing arrangement

Upon selecting a location, a stable platform, in which both machinery and workers could safely carry out the work, was erected with the use of Galvanized Iron pipes connected to each other to form a grid both parallel to the ground and the soil nailing surface. A rotary drilling machine was placed adjacent to the test nail location, and the drilling process commenced by placing the shaft of the drill perpendicular to the surface. This procedure was carried out until the shaft reached the desired depth. The soil nails placed within the drilled holes were galvanized (BS729) with a minimum coat thickness of 85microns or $610g/m^2$ on 25mm diameter tor steel reinforcement (BS 4449). Grade 500 QST high yield deformed bars of appropriate length with a cold rolled thread of at least 150mm (as such that a significant length would be protruding beyond the soil surface) were used. The soil nail to be grouted required a cover of 50mm. Thus, it was supported by 100mm diameter centralizers to ensure 50mm cover from the bored surface. The grouting procedure initiated, after the soil nail was placed in the bored hole and the grouted length was limited to 2.5 m in the bottom end of the borehole. A grouting pressure of 2 bar was used to maintain the necessary flow rate. The grout (complied with the provisions of BS12) included ordinary Portland cement mixed with Al powder 0.005 percent by weight of cement to prevent shrinkage.

Eight test nails were installed in 5m long bore holes, with grouted length of 2.5m. Grouting of short lengths was done following the guidance in Geoguide 7 - Guide for Soil Nail Design and Construction (2008) to ensure that the nails can be pulled out without causing tensile failure. The overburden heights at the centre of the grouted length at test locations are depicted on Figure 5. The locations of undisturbed box samples are also presented in the same figure.

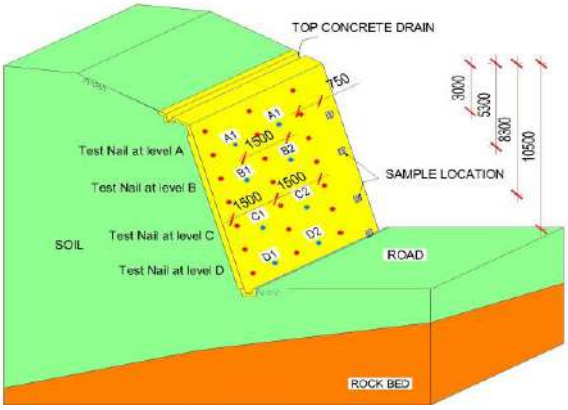

Figure 5: Locations of test nails and box samples

The jack used to pull the test nail was fixed to the nail as shown in Figure 6; the threads cut in the nails were used to tighten the grip of the loads supporting the apparatus, with the use of nuts. A dial gauge was then connected along the axis of nail to the apparatus in order to measure the amount of pullout and the dial gauge mounted to the jack was used to monitor load applied

Considering an average pullout resistance of $100kN/m^2$, the pullout load over the grouted nail length (2.5m) was estimated to be around 100kN (Design Load DL). Pressure was gradually applied on the jack, until the dial reached the required load. Tests were carried out in four loading cycle (FHWA 2003) having loading sequence of 0.5 Design Load (DL), 0.75DL, 1.0DL and 1.25DL.

Ultimately (after completion of the four cycles) the nail was loaded to the point of failure. Due to safety reasons, the dial gauge was removed in this final cycle. In this Final cycle, the pullout load on the nail was gradually increased using the jack as in the previous cycles until the load transferred started to decrease. This release of load signifies that the nail has reached the pullout capacity.

Displacements at different levels of loading in the initial cycles of the pullout loading are presented graphically in Figure 7 to Figure 10.

Figure 6: Apparatus used to pull the test nails

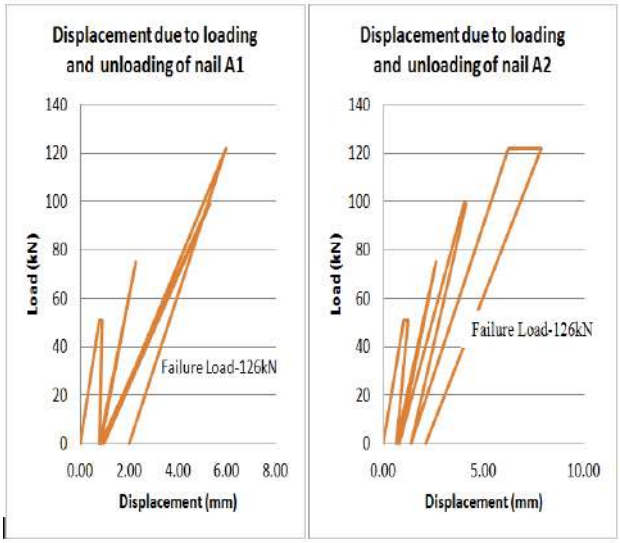

Figure 7: Displacement Vs Loading at Level A

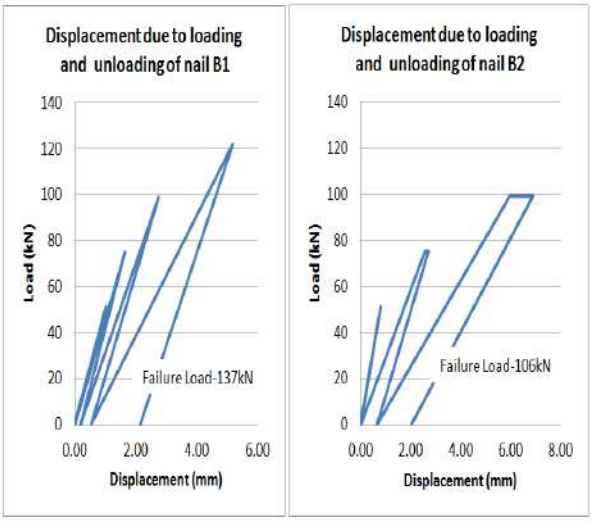

Figure 8: Displacement Vs Loading at Level B

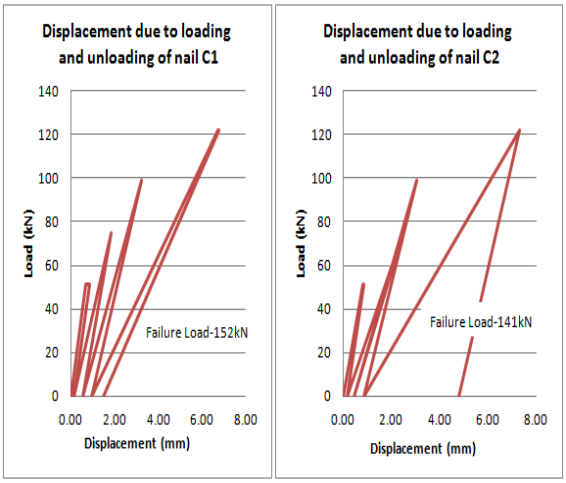

Figure 9: Displacement Vs Loading at Level C

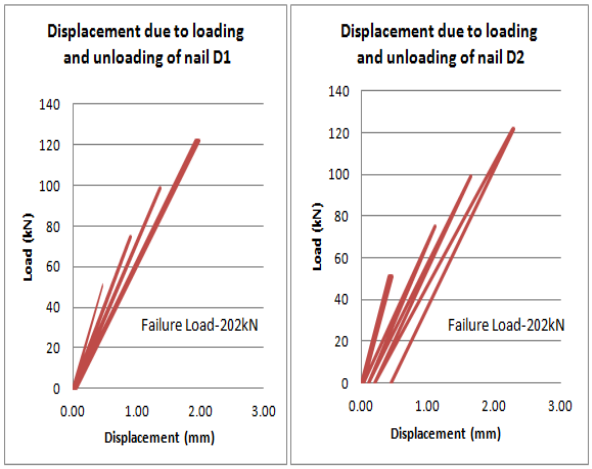

Figure 10: Displacement vs Loading at Level D

The measured pullout capacity in the ultimate cycle that was done to determine the ultimate pullout load is summarized in Table 1.

Table 1: Measured pullout capacity in the ultimate cycle

Location	Depth of overburden(m)	Measured Pull Out Capacity(kN)
A1	2.25	126
A2	2.25	126
B1	4.5	106
B2	4.5	137
C1	7.5	152
C2	7.5	141
D1	9.25	202
D2	9.25	202

Upon completion of the pullout test, the test nails were completely pulled out of the slope surface using heavy machinery, and the perimeters of the grouted bodies of the respective nails were measured, and the corresponding diameters were eventually calculated. It was observed that the average measured diameter of the grouted body was 22.6% greater than the drill hole diameter (116mm).

Figure 11: on site measurement of grouted body of pulled out test nail

4. DETERMINATION OF ENGINEERING PROPERTIES OF THE SOIL

The experimentally determined pullout resistances should be compared with the theoretical estimates made with currently used methods of estimation. Therefore it is necessary to obtain relevant shear strength parameters at close proximity to the test nails. Considering the variability of residual soils attempts were made to obtain undisturbed samples from all four test nail heights, namely A,B,C and D. The locations are presented in Figure 5. Under these conditions it was decided that box sampling would be the most appropriate technique. The, box samples of size 0.3mX0.3mX0.3m were eventually sealed using wax and polythene and safely transported to the laboratory.

Figure 12: Undisturbed box sample

4.1 Laboratory tests and Results

The samples transported to the laboratory were subjected to the Atterberg limit test, hydrometer test, sieve analysis, the direct shear test, and tests to obtain moisture content and bulk density. The results obtained through the aforesaid tests, are presented in Table 2, these results were used to calculate the theoretical pullout resistance.

Since the sample A was disturbed and could not be used, the soil parameters pertaining to sample B were used for calculation purposes of location A.

5. COMPARISON OF MEASURED AND COMPUTED PULLOUT RESISTANCE

The literature survey conducted provided information on number of different methods used at present by design engineers for the estimation of pullout resistance in soil nailing designs. Five of those methods were used in this study to estimate the pullout resistance. The methods are summarized in Table 3.

Methods 1 to 4 did not account for the presence of matric suction. They did not made any specific comment on the nature of shear strength parameters, i.e. whether they are saturated parameters or unsaturated parameters. Method 5, based on more recent research Gurpersaud (2010) has accounted for the matric suctions and allowed for dilation effects as well.

Table 2: Laboratory test results

Nail Location	A	B	C	D
C' (kPa)--Natural	20	20	48	10
C' (kPa)--Saturated	9	9	23	27
Φ'---Natural	33	33	16	44
Φ'---Saturated	33	33	16	44
Atterberg Limit				
Liquid Limit (LL)	65%	65%	77%	Non Plastic
Plastic Limit (PL)	39%	39%	39%	Non Plastic
Plastic Index (PI)	26%	26%	37%	-
Moisture content (W)	28.9%	28.9%	47.8%	14.1%
γ_{bulk} (kN/m3)	15.43	15.43	14.84	18.93
γ_{Sat} (kN/m3)	17.68	17.68	16.20	20.44
Percentage fines %	73.78	73.78	87.54	16.84
Percentage Sand %	26.22	26.22	12.46	80.16
Percentage Gravel %	0	0	0	3
Classification Symbol	MH	MH	MH	SM

During the laboratory testing shear strength parameters were obtained both under the insitu unsaturated condition and under the saturated conditions from three undisturbed box samples. The next task is to assign an appropriate set of parameters to different test locations. From the four box samples obtained tests could be conducted only on three samples namely; B, C and D.

It is necessary to have an estimate of matric suction to be used with Method 5. In the absence of any measured matric suction values a profile was assumed taking a maximum negative value of 100 kPa. The assumed profile is presented in Figure 13.

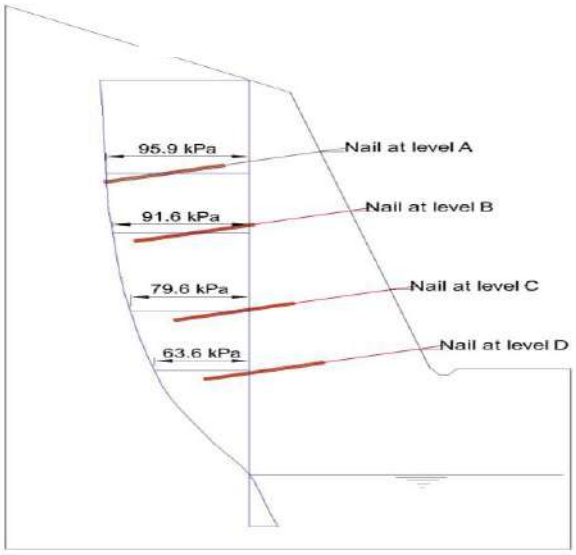

Figure 13: Assumed metric suction variation with elevation

Table 3: Different methods for estimation of pullout resistance

Method 01	**Schlosser and Guilloux** $T_L = Pc' + 2D_{eq}\sigma'_v\mu^*$ Where; T_L =ultimate pull-out resistance(kN/m) , C'=effective cohesion of the soil σ_v'=effective vertical stress calculated at the mid-point of the nail in the resistance zone, μ^*=coefficient of apparent friction of the soil (for granular soils, μ^* is usually taken to be equal to $\tan\phi'$, P=perimeter of the soil nail, D=diameter of the nail
Method 02	**Heymann et al.(1992)** $T_L = P(C' + \sigma'_N \tan\phi')$ Where; T_L =ultimate pull-out resistance(kN/m), P=perimeter of the soil nail, C= cohesion of the soil, σ_n=normal stress(assumed $\sigma_n = \sigma_v$ for the calculation)
Method 03	**Hansmann (1992)** $T_L = \pi DC' + 2DK_\alpha \sigma_v \tan\phi'$ Where; $K_\alpha = (1-\alpha/90)(1-K_0)$ $K_\alpha = (1-\alpha/90)(\sin\phi')$, α=cutting slope(15 degree) T_L =ultimate pull-out resistance(kN/m), D=diameter of the nail C'= effective cohesion of the soil, σ_v=effective vertical stress
Method 04	**According to HA 6894** $T_p = \pi D(C + \sigma_n \tan\phi)$ Where; $\sigma_n = (1+KL)\sigma_v/2$, $KL = (1+Ka)/2$, $Ka = (1-\sin\phi)/(1+\sin\phi)$, C= cohesion of the soil, T_p =ultimate pull-out resistance(kN/m), D=diameter of the nail, σ_n=normal stress
Method 05	**Gurpersaud(2010)** $Q_{f(us)} = \{(c_a + \beta\sigma'_z) + (u_a - u_w)(S^K)\tan(\delta+\psi)\}\pi dL$ $\beta = k\tan(\delta+\psi)$, $k = k_0 = 1 + (1-k_0)/2\, k_{0s}(1/\cos 2\theta)$ Where; $Q_{f(us)}$ =ultimate pull-out resistance(kN/m), β=Bjerrem-burland coefficient C_a=aperent cohesion of the soil, S=degree of saturation, K=fitting parameter(=1) σ_z'=effective vertical stress calculated at the mid-point of the nail in the resistance zone , ψ=dilation angle (taken10 and 20 degree), δ=interface friction angle L=effective length of the soil nail, d=diameter of the nail, θ=cutting slope

5.1 Estimation of pullout capacity with unsaturated and saturated shear strength parameters

Method 1 to Method 4 for the estimation of pullout resistance used shear strength parameters without specifying whether they are saturated or unsaturated parameters. However, according to the prevailing site conditions all the test nails were under unsaturated conditions. As such, the pullout resistance was estimated using Methods 1 to Method 4 using the determined corresponding unsaturated shear strength parameters in the equations. Method 5 accounts for matric suction as well as dilation effects. The shear strength parameters c' and ϕ' corresponding to the expression of Method 5 are therefore saturated parameters. Hence, pullout resistance values were estimated by method 5 using the saturated parameters and estimated matric suction and angle of dilation. The values obtained are summarized in Table 4 and graphically presented in Figure 14.

The estimated values as a percentage of corresponding experimentally observed values are presented in Table 5.

Method 1 to Method 4 would result in values presented in Table 6 if saturated shear strength parameters were used in the estimate of pullout resistance. The estimated values as a percentage of corresponding experimentally observed values are presented in Table 7. Obviously, these values are much lower than the values computed under unsaturated condition and are much lower than the actual observations.

Table 4: Measured and estimated pullout capacity

Pull out capacity kN/m							
Overburden height (m)	Measured	Method 01	Method 02	Method 03	Method 04	Method 05	
						for Ψ =10°	for Ψ =20°
4.57	50.40	17.91	23.98	16.95	21.03	31.24	37.38
4.57	50.40	17.91	23.98	16.95	21.03	31.24	37.38
6.46	54.80	22.32	30.89	20.95	26.73	34.76	40.62
6.46	42.40	22.32	30.89	20.95	26.73	34.76	40.62
9.00	60.80	26.38	31.45	25.97	29.94	34.15	40.05
9.00	56.40	26.38	31.45	25.97	29.94	34.15	40.05
10.92	80.80	49.96	76.40	44.59	54.53	57.76	64.10
10.92	80.80	49.96	76.40	44.59	54.53	57.76	64.10

Graphs of measured-a and measured-b represent the measured pullout capacity behavior.

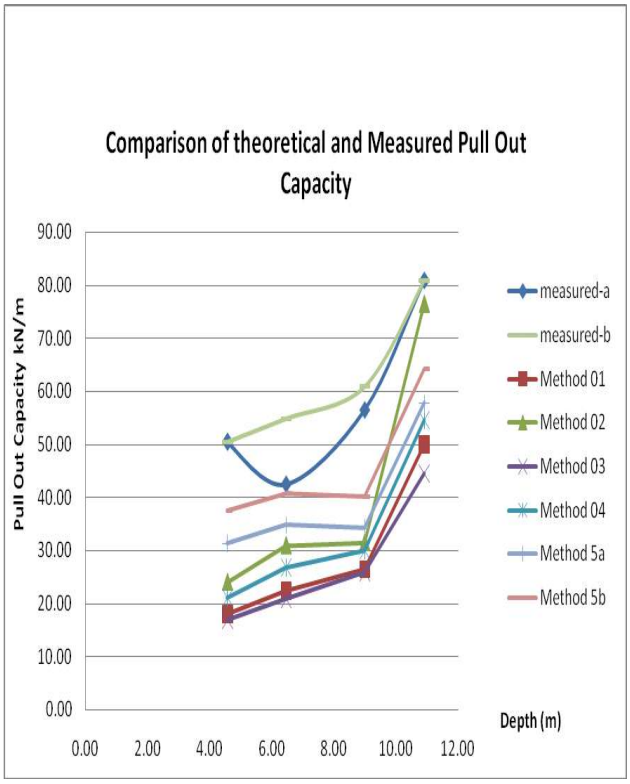

Figure 14: Theoretical and measured pullout capacity

Table 5: .Percentage comparison-Theoretical & Measured

Pull out capacity for saturated condition kN/m					
Location	Depth (m)	Method 01	Method 02	Method 03	Method 04
A1	4.57	15.45	22.40	14.35	19.02
A2	4.57	15.45	22.40	14.35	19.02
B1	6.46	20.50	30.33	18.93	25.55
B2	6.46	20.50	30.33	18.93	25.55
C1	9.00	18.08	23.62	17.64	21.97
C2	9.00	18.08	23.62	17.64	21.97
D1	10.92	59.86	88.41	54.05	66.25
D2	10.92	59.86	88.41	54.05	66.25

Table 6: Estimated pullout capacity (saturated)

Percentage of estimated pull out capacity as a measured capacity						
					Method 05	
Overburden height (m)	Method 01	Method 02	Method 03	Method 04	for Ψ =10°	for Ψ=20°
4.57	35.54	47.57	33.62	41.73	61.98	74.17
4.57	35.54	47.58	33.62	41.73	61.98	74.17
6.46	40.72	56.37	38.23	48.77	63.43	74.12
6.46	52.64	72.85	49.41	63.04	81.98	95.80
9.00	43.39	51.73	42.71	49.25	56.17	65.87
9.00	46.77	55.76	46.04	53.09	60.55	71.01
10.92	61.83	94.55	55.19	67.49	71.49	79.33
10.92	61.83	94.55	55.19	67.49	71.49	79.33

Table 7: Percentage of estimates pullout capacity for saturated condition as a measured capacity

Percentage of estimated pull out capacity as a measured capacity					
Location	Depth (m)	Method 01	Method 02	Method 03	Method 04
A1	4.57	30.7	44.4	28.5	37.7
A2	4.57	30.7	44.4	28.5	37.7
B1	6.46	37.4	55.3	34.5	46.6
B2	6.46	48.3	71.5	44.6	60.3
C1	9.00	29.7	38.8	29.0	36.1
C2	9.00	32.1	41.9	31.3	39.0
D1	10.92	74.1	109.0	66.9	82.0
D2	10.92	74.1	109.0	66.9	82.0

All estimates under unsaturated conditions were increased (Table 8) by 22.6%, corresponding to observed perimeter increase. However, the comparison illustrates that even these values are lower than the measured pullout resistance except last nail level of method 02. The measured pullout resistance is plotted against the overburden height in Figure 15

Table 8: Estimated pullout capacities considering measured effective diameter of nails

Pull out capacity kN/m							
						Method 05	
Overburden height (m)	Measured	Method 01	Method 02	Method 03	Method 04	for Ψ =10°	for Ψ =20°
4.57	50.40	21.96	29.40	20.78	25.78	38.30	45.83
4.57	50.40	21.96	29.40	20.78	25.78	38.30	45.83
6.46	54.80	27.36	37.87	25.68	32.77	42.62	49.80
6.46	42.40	27.36	37.87	25.68	32.77	42.62	49.80
9.00	60.80	32.34	38.56	31.83	36.71	41.87	49.10
9.00	56.40	32.34	38.56	31.83	36.71	41.87	49.10
10.92	80.80	61.25	93.67	54.67	66.85	70.81	78.59
10.92	80.80	61.25	93.67	54.67	66.85	70.81	78.59

The measured pullout resistance is plotted against the overburden height in Figure 15.

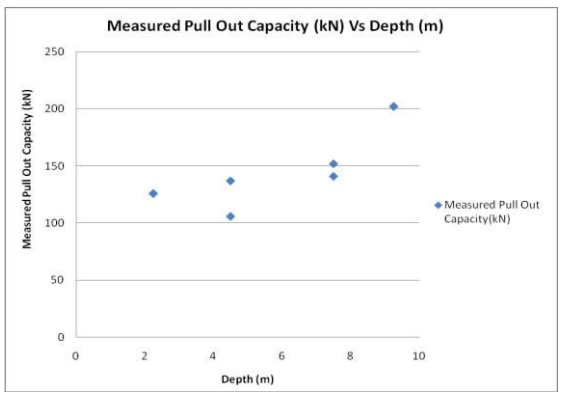

Figure 15: Measured pullout capacity with overburden height

5.2 Comparison of pullout and direct shear test results

Both direct shear test and pullout test mechanisms are having similar behavior where shear resistance was mobilizing gradually with the shear displacement. Hence a direct comparison of shear stress Vs displacement behavior during tests could provide some insight into the pullout mechanisms. As such, it was decided to plot the two test results together. A similar comparison was done by Chu and Yin (2005). The loads at different stages in the pullout tests were converted to shear stresses by dividing it by the effective nail surface area. The pullout test results were compared with direct shear test B, C and D (unsaturated). In order to obtain a direct comparison of two types of plots, both the direct shear test results and the pullout resistance test results were normalized by dividing by the applied normal stress or the overburden stress. The respective normalized values obtained have been presented in Figure 16, Figure 17 and Figure 18. Even under this normalized condition the pullout resistance values generally plotted above the direct shear test values.

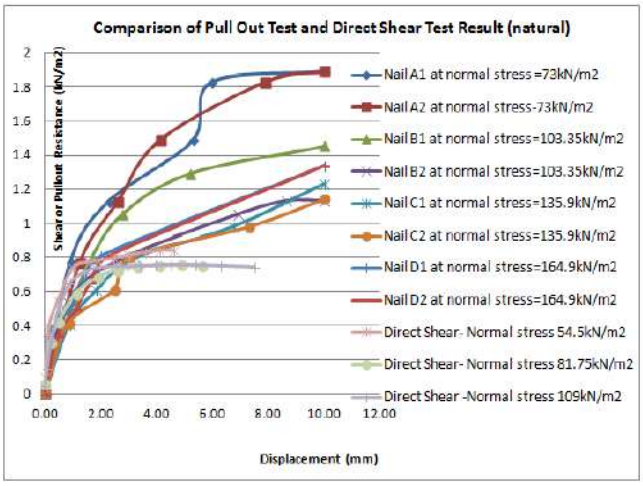

Figure 16: Normalized Pullout Vs Direct Shear test (B – natural)

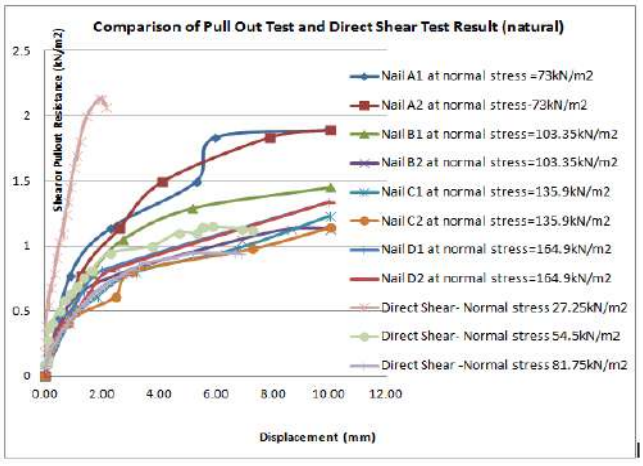

Figure 17: Normalized Pullout Vs Direct Shear test (C natural

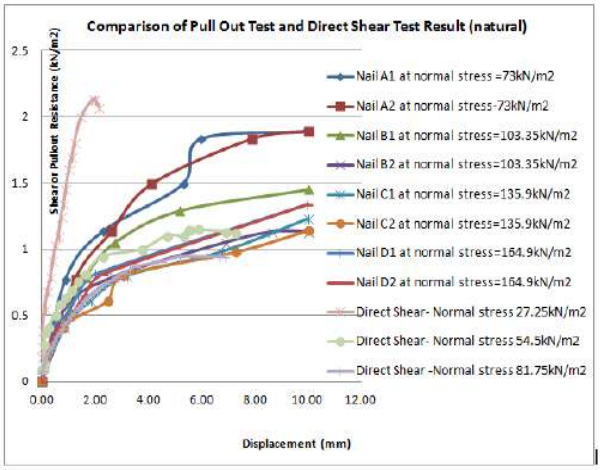

Figure 18: Normalized Pullout Vs Direct Shear test (D – natural)

6. CONCLUSIONS AND RECOMMENDATIONS

6.1 Variation of pull out capacity with depth

It is evident that the measured pull out capacity that it increases with the depth, although some researchers have commented that pullout resistance is independent with the depth.

All equations used for the estimation of pull out capacity suggest that it is directly proportional to the overburden pressure (which is a dependent variable of depth).

6.2 Effective diameter of soil nails

The average diameter of the grouted nail has been increased by 22.6%.This could be due to anomalies in drilling or penetration of grout into the soil under the grouting pressure. Nevertheless very high grouting pressures are not normally used in soil nailing. This is an area that needs further studies.

6.3 Comparison of the estimated and measured pullout resistance

The comparison of the measured pullout resistance with the predictions done with different methods currently in use clearly indicated that all the current methods underestimate the pullout capacity. By accounting for the,

- Unsaturated condition that prevail
- Possible dilation during pullout
- Possible increase of drill hole diameter due to grout pressure,

values much closer to the experimentally determined values can be obtained. In here the matric suction values were assumed as it could not be measured. If much higher matric suction values have prevailed and used in the analysis the computed pullout resistance values would be increased. The fifth method by Gurpersaud (2010)

accounts for matric suction and dilation. When the predictions were done accounting for both matric suction (using an assumed suction profile) and dilation the predictions were much closer although still lower than the experimental observations.

6.3.1 Comparison of stress- strain curves of pull out and the direct shear tests

In both the direct shear test and the pullout test shear resistance is mobilized along a failure surface as the induced deformation increases. As such, the stress strain curves of the two tests are comparable.

The test results were compared after normalizing with the normal stress or overburden stress. Pullout tests were compared separately with the direct shear tests done with undisturbed samples obtained from locations B, C and D. When the comparisons were done with direct shear test results of samples B and C all the normalized pullout test were above the direct shear tests. The stress-strain curves of pullout test showed a strain hardening type effect whereas the direct shear test results showed a reduction in stress after reaching the peak value.

The undisturbed sample D was more granular with a high angle on internal friction. When the normalized pullout test results were compared with the normalized direct shear test results of sample D, the direct shear test results were plotted above the pullout test results. All undisturbed samples B, C and D were obtained at the face of the nailed slope. The test nails were installed over the last 2.5m length of the hole drilled for a 5m length.

The change in the soil properties further into the slope over this 5m perhaps to a less weathered condition could cause an increase in the pullout resistance from the computed values. Therefore, to make an accurate prediction of the pullout resistance it is necessary to test samples obtained further inside the slope closer to the resistant zones in the nails.

6.4 Concluding comment on the comparisons

All the comparisons indicate that the matric suction and dilation have a contribution to the pullout resistance.

The variability of the soil should also be accounted. The test samples used for the laboratory tests were at the face of the slope and much less weathered (or more frictional) soils could be encountered further into the slope where pullout resistances of the nails are mobilized.

Thus, it is necessary to get sufficient samples to get a good assessment of special variability of the shear strength. However, there are practical limitations on this.

6.5 Recommendations for further research

The influence of matric suction on the pullout resistance should be established. In an identified test slope, pullout resistance measurements should be done under highly unsaturated conditions as well as under induced saturated conditions. (eg: sprinkling of water). These tests should be done along with the matric suction measurements in the resistant zone closer to the nail locations.

The variability of the soil conditions over the length of the nail should be well established by taking sufficient number of samples. This could be done initially as a large laboratory model to be followed by a instrumented field study.

With such studies, the contribution of matric suction to the pullout resistance and the reduction of the pullout resistance with the loss of matric suction could be established. After studying the rainfall pattern in a given location a design rainfall (say 100 year) could be established and incorporating that into an infiltration analysis a design matric suction profile could be derived. This matric suction profile could be used in the estimation of pullout resistance. The formula proposed by Gurpersaud (2010) could be further developed with these data

ACKNOWLEDGEMENTS

It is our pleasure to take this opportunity to thank all those who have been supportive in this to me to successfully complete this research. Cooperation extended by the laboratory staff of the Geotechnical Engineering division of the Department of Civil Engineering, University of Moratuwa, is greatefully acknowledged. The encouragement given by the Management of the Central Engineering Consultancy Bureau (CECB) and support extended by the laboratory staff of CECB during the laboratory testing is also gratefully acknowledged. Assistance given by the Engineering & Laboratory Services (Pvt) Ltd while performing on field tests is highly appreciated.

Finally, we would like to thank the site staff of the Operation Theatre Complex Building, Teaching Hospital, Kegalle for voluntarily involving themselves in the field during various stages of this research.

REFERENCES

1. BS 12 – Specifications for Portland cement – British Standard Institute.
2. BS 729 – Specification for hot dip galvanized coatings on iron and steel articles - British Standard Institute.
3. BS 4449 – Steel for reinforcement of concrete. - British Standard Institute.
4. Burland, J. B. 2002. Reliability of soil nailed slopes in Hong Kong, Geotechnical Engineering Office, Hong Kong Government, Hong Kong.

5. Byrne, R. J.,Cotton, D., Porterfield, J.,Wolschlag, C., and Ueblacker, G.1998. “Manual for design and construction monitoring of soil nail walls.” Rep. No.FHWA-SA-96-069R.
6. Cartier, G., and Gigan, J. P. 1983. “Experiments and observations on soil nailing structures.” Proc., European Conf. on Soil Mechanics and Foundation Engineering, 473–476.
7. Chai, X.J. and Hayashi, S. and Du, Y.J. 2004.Contribution of dilatancy to pullout capacity of nails in sandy clay. In Soil Nailing and Stability of Soil and Rock Engineering, Nanjing, China, pp. 73-80.
8. Chu, L.-M., and Yin, J.-H. 2005. “Comparison of interface shear strength of soil nails measured by both direct shear box tests and pullout tests.” J. Geotech. Geoenviron. Eng., 131(9), 1097–1107.
9. FHWA. 1993. Recommendations clouterre 1991 (English translation). Report on the French national research project clouterre, FHWA-SA-93-026. Federal Highway Administration, Washington, DC.
10. FHWA 2003. Geotechnical Engineering Circular No. 7 - Soil Nail Walls. Federal Highway Administration, US Department of Transportation, Washington, D.C., USA, Report No. FHWA0-IF-03-017, 210 p.
11. Franzen, G. 1998. “Soil nailing a laboratory and field study of pull-out capacity.” Ph.D. thesis, Chalmers Univ. of Technology, Göteborg, Sweden.
12. Franzen, G., and Jendeby, L. 2001. “Prediction of pullout capacity of soil nails.” Proc., 15th Int. Conf. on Soil Mechanics and Geotechnical Engineering, Vol. 3, Balkema, Rotterdam, The Netherlands, 1743–1748.
13. Geoguide 7 2008 – Guide to Soil Nail Design and Construction, Geotechnical Engineering office, The government of Hong Kong
14. Gurupersaud Naresh 2010, The influence of matric suction on the pull-out capacity of Grouted soil nails, A Thesis submitted to the Carleton University, Ottawa-Carleton, for partial fulfillment for the Degree of Master of Applied Science.
15. HA68/94. 1994. Design methods for the reinforcement of highway slopes by reinforced soil and soil nailing technique. Road Authorities in England, Welsh, Scotland and Northern Ireland.
16. Heymann, G., Rhode, A. W., Schwartz, K., and Friedlaender, E. 1992.“Soil nail pullout resistance in residual soils.” Proc., Int. Symp. On Earth Reinforcement Practice, Vol. 1, Balkema, Rotterdam, The Netherlands, Kyushu, Japan, 487–492.
17. Junaideen, S.M., Tham, L.G., Law, K.T., Lee, C.F. and Yue, Z.Q. 2004. Laboratory study of soil-nail interaction in loose completely decomposed granite, Canadian Geotechnical Journal, 41(2): 274-286.
18. Li, K. S., and Lo, S. R. 2007. “Discussion of comparison of interface shear strength of soil nails measured by both direct shear box tests and pullout tests by Lok-Man Chu and Jian-hua Yin.” J. Geotech. Geoenviron.Eng., 133(3), 344–346.
19. Milligan, G. W. E., and Tei, K. 1997. “The pullout resistance of model soil nails.” Soils Found., 38(2), 179–190.
20. Pradhan, B. 2003. Study of the pull-out behaviour of soil nails in completely decomposed granite fill. M.Pill thesis, The University of Hong Kong. Pradhan
21. Pradhan, B., Tham, L. G., Yue, Z. Q., Junaideen, S. M., and Lee, C. F.2006. “Soil-nail pullout interaction in loose fill materials.” Int. J.Geomech., 6(4), 238–247.
22. Plumelle, C. Schlosser, F., Oclage, P., and Knochenmus, G. 1990. “French National Research Project on Soil Nailing: CLOUTERRE,” Geotechnical Special Publication No. 25, American Society of Civil Engineers, pp. 660-675.
23. Powell, G.E. and Watkins, A.T. 1990. Improvement of marginally stable existing slopes by soil nailing in Hong Kong. In Proceedings of the International 16. Reinforced Soil Conference, Glasglow, U.K., pp. 241-247.
24. Schlosser, F. and Guilloux, A. 1982. “Le frottement dens les sols. Revue Francaise de.” Géotechnique. 16:65-77(1981)
25. Schlosser, F. (1983). Schlosser, F., Jacobsen, H.M., and Juran, I. 1983. "Soil reinforcement, General Report- Specialty Session 5." Proceedings of the 8th International Conference Soil Mechanics and Foundations Engineering, Helsinki, 1159-1180.
26. Seo Hyung- Joon, Kyeong-Han Jeong, Hagseok Choi and In-Mo Lee 2012 , Pullout resistance Increase of Soil Nailing Induced by Pressurized Grouting, ASCE Journal of the Geotechnical and Geo-environmental Engineering, Vol 138, No 5 May 2012; pp 604-613
27. Sivakumar,. and Singh, V.P. 2010. Soil nails field pullout testing: evaluation and applications. International Journal of Geotechnical Engineering, 4: 13-21.
28. Su, L.J., Chan, T.C.F., Shiu, Y.K., and Cheung, T. and Yin, J.H. 2008. Influence of degree of saturation on soil nail pullout resistance in compacted completely decomposed granite fill. Canadian Geotechnical Journal, 44(11): 1314-1328.
29. Yeo, K. C., Lo, S. R., and Yin, J. H. 2007. “Installation method and overburden pressure on soil nail pullout test.” New Horizons in Earth Reinforcement. Proc., 5th Int.Symp. on Earth Reinforcement, J. Otani, Y. Miyata, and T. Mukunoki, eds., Taylor and Francis, Kyushu, Japan,321–327.
30. Yin, J.H. and Su, L.J., 2006. An innovative laboratory box for testing nail pull-out resistance in soil, ASTM Geotechnical Testing Journal, 29: 1 - 11
31. Zhang, L.L., Zhang, L.M., and Tang, W.H. 2009. Uncertainties of field pullout resistance of soil nails, Journal of Geotechnical and Geo-environmental Engineering, 135(7): 966-973.